Global and Planetary Change 230 (2023) 104260

Contents lists available at ScienceDirect

Global and Planetary Change

journal homepage: www.elsevier.com/locate/gloplacha

Research paper

Influence of climate and non-climatic attributes on declining glacier mass budget and surging in Alaknanda Basin and its surroundings

Atanu Bhattacharya [a,**], Kriti Mukherjee [b,*], Owen King [c,i], Shubhendu Karmakar [a,d], S.N. Remya [e], Anil V. Kulkarni [f], Jan Kropáček [g], Tobias Bolch [c,h]

[a] Department of Earth Sciences & Remote Sensing, JIS University, Kolkata, India
[b] Cranfield Environmental Centre, Cranfield University, Bedford, UK
[c] School for Sustainable Futures, University of St. Andrews, UK
[d] Regional Meteorological Centre Kolkata, India Meteorological Department (IMD), India
[e] School for Sustainable Futures, Amrita Vishwa Vidyapeetham, Kerala, India
[f] Divecha Centre for Climate Change, Indian Institute of Science (IISc), Bangalore, India
[g] Department of Physical Geography & Geoecology, Charles University, Czech Republic
[h] Institute of Geodesy, Graz University of Technology, A-8010 Graz, Austria
[i] School of Geography, Politics and Sociology, Newcastle University, Newcastle upon Tyne, UK

ARTICLE INFO

Editor: Prof. Liviu Matenco

Keywords:
Glacier mass budget
Glacier surge
Gridded climate reanalysis data
Non-climatic attributes
Glacier dynamics

ABSTRACT

Globally glaciers are rapidly shrinking, endangering the sustainability of melt water and altering the regional hydrology. Understanding long-term glacier response to climate change and the influence of non-climatic attributes like morpho-topographic factors on ice loss is of high relevance. Here we estimate the multi-temporal mass balance of 445 glaciers in the upper Alaknanda basin and neighboring transboundary glaciers using optical stereo imageries from 1973 to 2021. Our measurements indicate a mean annual area change rate of −1.14 ± 0.07 km^2 a^{-1} and a geodetic glacier mass balance of −0.34 ± 0.08 m w.e. a^{-1} from 1973 to 2020, leading to an overall mass loss of 12.9 ± 1.7 Gt, that accounts for up to 0.036 ± 0.006 mm of sea level rise. Before 2000 (1973–2000), the mean regional glacier mass loss rate was −0.30 ± 0.07 m w.e. a^{-1}, which increased to −0.43 ± 0.06 m w.e. a^{-1} during 2000–2020. ERA5 Land reanalysis data showed a summer and annual temperature rise of ~0.6 °C and ~ 0.5 °C respectively in recent time period (2015–2020) and consequent strong mass loss (−0.68 ± 0.09 m w.e. a^{-1}). In addition to climatic influence, glacier morphometry, topographic features and uneven debris cover distribution further impacted the regional and glacier specific mass balance. Our multi-temporal observation from space also emphasized that though the glaciers in this region experienced an increasing mass loss but a strong heterogeneous glacier specific response, like surging and dynamic separation of glacier, are also evident that was not captured by the available long-term global elevation change grids. Among all the climatic and non-climatic attributes, we identified summer temperature having most significant influence over glacier mass budget in this region, with a mass balance sensitivity of −0.6 m w. e. a^{-1} $°C^{-1}$. Hence, knowing the mean summer temperature will help to predict the mass balance for any intermediate year for this region. If such climatic trend continues, smaller glaciers are likely to disapear in coming decades. Similar studies in other parts of the world and on specific glaciers can reveal links with climate factors, reconstruct mass balance, and enhance comprehension of glacier response to climate change. Our geodetic mass balance estimates will improve the estimation of meltwater run-off component of the hydrological cycle in this part of the Himalaya, which could be used to calibrate/validate glacier mass balance models.

1. Introduction

Approximately 800 million people in Indo-Gangetic plain depend on snow and glacier melt as their primary source of drinking water and irrigation (Gornall et al., 2010; Biemans et al., 2019; Pritchard, 2019; Immerzeel et al., 2020; Kulkarni et al., 2021). Meltwater run-off,

* Corresponding Author.
** Corresponding Author.
E-mail addresses: atanudeq@gmail.com (A. Bhattacharya), Kriti.Mukherjee@cranfield.ac.uk (K. Mukherjee).

https://doi.org/10.1016/j.gloplacha.2023.104260
Received 17 February 2023; Received in revised form 15 August 2023; Accepted 28 September 2023
Available online 29 September 2023

draining from the large concentration of glaciers in the Himalaya-Karakoram (HK) region, is not only important for downstream communities but also represents a significant component of the hydrological cycle (Bolch et al., 2012). However, mountain glaciers in the Asian Water Tower and all over the world are highly vulnerable to ongoing climate change (Viviroli et al., 2011; Immerzeel et al., 2020). Glaciers here have lost mass at an accelerated rate during the last decades (Zemp et al., 2019; Hugonnet et al., 2021; Bhattacharya et al., 2021) and projected increases in global temperature will exacerbate the rate of ice loss (Kraaijenbrink et al., 2017; Bolch et al., 2019; Hock et al., 2019; Rounce et al., 2020). Whilst glacier meltwater yield may currently be increasing due to glacier wastage, the output of freshwater from the high mountain cryosphere will not be sustained in the future as glacier volume reduces, bringing into question the sustainability of this vital water resource in coming decades (Kraaijenbrink et al., 2017; Huss and Hock, 2018; Bolch et al., 2019; Rounce et al., 2020). In the Indian subcontinent, multiple climate projection models (Chaturvedi et al., 2012; Kulkarni et al., 2020) indicate an increase of temperature and annual precipitation, but decrease in snowfall, which will make glaciers in this region susceptible to further melt. Based on the annual glacier run-off projections by Rounce et al. (2020), peak water in the monsoon fed Ganges basin will reach around 2030, followed by a declining glacier run-off. This means reduced supply (32%–41%) of end of summer fresh water for a larger than currently existing population (Kraaijenbrink et al., 2017; Huss and Hock, 2018; Bolch et al., 2019; Rounce et al., 2020). In addition to climatic factors such as temperature and precipitation, many other non-climatic factors have been shown to influence glacier mass balance in the HK region, including glacier hypsometry (Mcgrath et al., 2017), ice dynamics (Clarke et al., 2015; Mukherjee et al., 2022), debris cover fraction and thickness (Salerno et al., 2017; Rounce et al., 2020), presence of supra- and proglacial lakes (Brun et al., 2019; King et al., 2019), glacier accumulation regime and glacier surges (Banerjee and Shankar, 2013; Guillet et al., 2022). Detailed, long-term records of glacier mass changes are crucial to improve our understanding of regional variability of glacier response to climate change, and better constrain the glacier mass balance models to estimate glacier run-off at finer temporal resolutions.

The Alaknanda basin in the Garhwal Himalaya, occupying ~800 km^2 glacierised area (Remya et al., 2020, 2022) is one of the important sources of freshwater for its downstream populations. Meltwater from these glaciers sustains the Alaknanda River. Glaciers in this region have undergone significant area loss (Bhambri et al., 2011; Remya et al., 2020, 2022; Mishra et al., 2022) and increase in debris cover fraction (Mishra et al., 2022) over the last decades. The glacier area loss at basin scale in this region is also affected by the climatic and several non-climatic attributes (Remya et al., 2020, 2022; Mishra et al., 2022).

Despite the considerable concentration of glaciers in this region, spatially resolved multi-temporal glacier mass balance datasets are not available to aid our understanding of the direct impact of the ongoing climate variability on the cryosphere in the region. Recent studies investigated geodetic glacier mass budget since 2000 (Bandyopadhyay et al., 2019; Bhambri et al., 2023) and reported mass loss (-0.32 ± 0.05 m w.e. a^{-1} for 2000–2014 and -0.28 ± 0.08 m w.e. a^{-1} for 2000–2017 respectively). More detailed studies document the consistent decline in glacier mass budgets over multi-decadal time periods along the Himalayan region (Bolch et al., 2011; Azam et al., 2016; Azam et al., 2018; Mukherjee et al., 2018; King et al., 2020) and across the wider HMA (Brun et al., 2017; Shean et al., 2020; Bhattacharya et al., 2021; Hugonnet et al., 2021). These studies elude to consider temporal and spatial mass loss heterogeneity which does not always clearly reflect local climate trends, which emphasizes the need to look beyond climatic factors to understand variability in glacier behaviour in near future.

Keeping the above points in mind, in this study we examined the response of the glaciers in the Alaknanda Basin and its surroundings by analyzing a variety of remotely sensed datasets. The specific aims of this study are the following:

- Estimate multi-temporal (1973–2020) geodetic mass budget for the glaciers of our study region.
- Investigate the dominant climate drivers (temperature, precipitation, snowfall) which are affecting glacier mass budget.
- Calculate mass balance sensitivity using multi-temporal mass budget and climate data.
- Explore the potential impact of non-climatic factors such as, glacier morphometry, topographic features and influence of debris cover, on the regional glacier mass budgets.
- Identify and investigate heterogeneous glacier specific response, such as glacier surge and dynamic separation of glaciers in our study region.

2. Study area

The Alaknanda Basin in the Garhwal Himalaya is a part of Uttarakhand state of India (Fig. 1) and is located between the latitude and longitude of 30.58°-31.12°N and 79.19°-79.86°E respectively (Nainwal et al., 2008). The Alaknanda River, one of the primary headstreams of the Ganga River, is the main river system in this basin and also serves as a crucial water source for millions of people living in Uttarakhand and downstream regions. Additionally, the region has an extreme religious significance, including some Hindu religious sites such as Badrinath, Hemkund Sahib, Joshimath. In addition, Alaknanda River is considered sacred by devotees who take dips in its water to cleanse themselves spiritually. The Alaknanda River originates from the Satopanth (SPG) and the Bhagirath Kharak (BKG) glaciers, joins the Saraswati River near Mana Village and finally connects the Bhagirathi River, another headstream of the river Ganga, near Devprayag. Glaciers in this region are fed by the Indian summer monsoon and winter westerlies (Thayyen and Gergan, 2010; Bhambri et al., 2011). The average annual temperature fluctuated between −7.0 °C and -4.2 °C between 1973 and 2021, according to ERA5 Land reanalysis data. The mean winter and summer temperature was estimated as −13.9 °C and 3.9 °C respectively during the observation period. Maximum snowfall was observed during December to March (Dobhal et al., 2008). There are no meteorological stations in the central Alaknanda Basin. Two stations Mukhim (~1981 m a.s.l) and Joshimath (~1650 m a.s.l) are located at ~100 km south west and ~40 km south of the BKG & SPG which are maintained by the India Meteorological Department (IMD). The average annual precipitation recorded in Joshimath and Mukhim station were ~1100 mm (1959–2013) and ~1622 mm (1973–2007), respectively (Kumar et al., 2017a, 2017b). The maximum and minimum mean air temperature was observed during June–July (~19 °C) and January (~8.0 °C) respectively at Mukhim Station.

Here, we expanded our study region (Fig. 1) beyond the Alaknanda Basin and included few nearby glaciers (located on the Tibetan Plateau and nearby the Saraswati Basin) within the same dataset that displayed different behaviour and discuss our results based on whole study area. We examined the behaviour of ~445 glaciers which occupied ~785.5 ± 23.2 km^2 of glaciated area with a median elevation range between ~3700–7686 m above sea level (a.s.l), estimated using the Advanced Spaceborne Thermal Emission and Reflection Radiometer (ASTER) Global Digital Elevation Model (GDEM) of 2000.

3. Dataset

We used a variety of satellite images with resolutions ranging from 0.5 m to 30 m (Supplementary Table 1) to delineate glacier boundaries and generate DEMs from different time periods between 1973 and 2020. We also considered published time series of glacier surface velocity estimates (Gardner et al., 2019; Friedl et al., 2021) and global debris thickness maps (Rounce et al., 2021) to understand glacier response over a similar period. Additionally, we considered Randolph Glacier Inventory (RGI V6.0) (Pfeffer et al., 2014) as the baseline representation of the glacierized area.

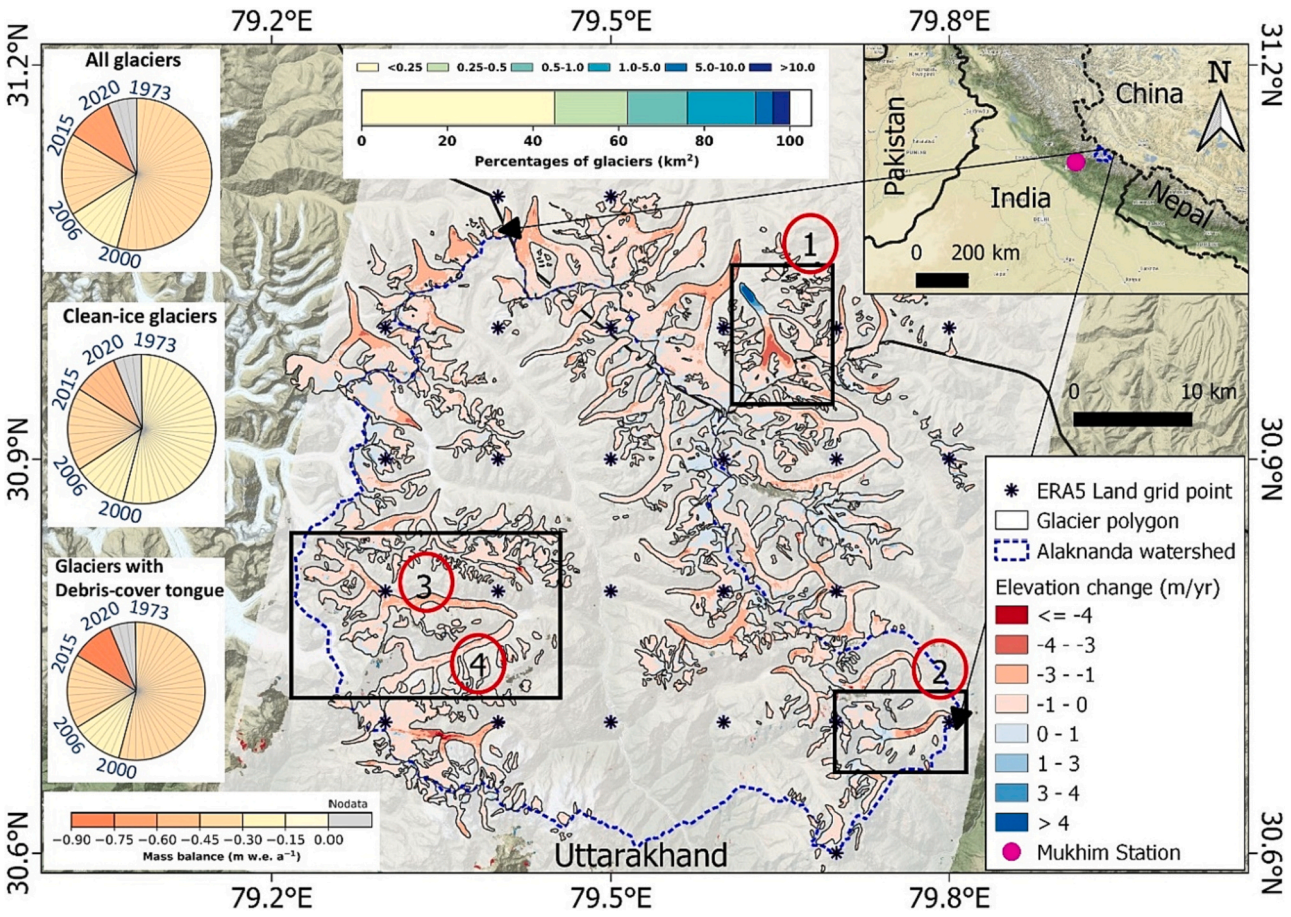

Fig. 1. Location of the investigated glaciers in Alaknanda Basin and its surrounding (1: Surge glacier RGI60–14-26,971; 2: Raj Bank RGI60–15-06559; 3: Bhagirath Kharak Glacier RGI60–15.07122/BKG; 4: Satopanth Glacier RGI60–15.07122/SPG) and mean glacier surface elevation changes for 2000 to 2020 period. Overall, debris covered and clean-ice glacier multi-temporal mass budgets (m.w.e. a^{-1}) are presented by left side pie diagrams. Glacier area distribution is represented by upper bar diagram. Approximately, 44% of the glaciers are <0.25 km^2.

3.1. Satellite images

For regional glacier analysis we used stereo imageries from the Hexagon KH-9 Mapping Camera (7.6 m), ASTER (15 m) and HMA DEMs (8 m) (Shean et al., 2016), developed from WorldView-1/2/3, Quickbird-2 and GeoEye-1 stereo sensors. Additionally, we used very high resolution Pléiades 1B stereo products (0.5 m), PlanetScope (~3.7 m) and Sentinel-2 (10 m) data for glacier scale investigation. Corresponding orthorectified images and Landsat data (30 m and 15 m) at various time periods were used to investigate temporal changes in glacier area. Furthermore, we used ice product (ATL06) from photon-counting Lidar altimeter ATLAS on board Ice, Cloud, and Land Elevation Satellite-2 (ICESat-2) which was launched by NASA in September 2018, to document changes in surface geometry of the surging glacier during the period 2019–2023. We also used Shuttle Radar Topographic Mission (SRTM) 3-arc sec (void) and SRTM-1 arc sec (non-void) DEMs for generation of DEMs from stereo optical data and coregistration of DEMs respectively.

3.2. Climate data

We evaluated the influence of several climate drivers (2 m temperature, total precipitation and snowfall i.e. solid precipitation) at regional scale by using ERA5 Land (~9 km spatial resolution) reanalysis data (Muñoz-Sabater et al., 2021) to improve our understanding of the response of glaciers to a changing climate. We primarily chose ERA5 Land over other reanalyses datasets (e.g. HAR V2) as it offers a time series of comparable length to our geodetic observations. A total of 30 grid points (Fig. 1) were used for the whole ~3180 km^2 area. To validate ERA5 Land data we also examined long term (1973–2007) climate data (temperature and precipitation) from Mukhim weather station (Fig. 1).

3.3. Non-climatic data

3.3.1. Morphometry data

Individual glaciers' morphometry data, such as, glacier elevations, mean slope, aspect and median elevation were derived from the ASTER Global Digital Elevation Model (GDEM).

3.3.2. Glacier surface velocity data

We used two sets of velocity data derived from optical (ITS_LIVE) and microwave (Sentinel-1) images. The annual median velocity field from the Landsat family of optical data (ITS_LIVE) was estimated for approximately 95% of glacier area across HMA from 1985 to 2018 using the AUTO_RIFT algorithm (Gardner et al., 2019). The velocity field derived from coarser Landsat (Landsat-5 and older) dataset has higher uncertainties in lower ablation regions (Dehecq et al., 2019). Therefore, we considered ITS_LIVE velocity field for the year 2000–2018. Velocity fields derived from Sentinel-1C-band SAR dataset (Strozzi et al., 2002; Friedl et al., 2021) after 2018 were also used to analyze individual glacier dynamics and extend observations towards the present day.

3.3.3. Debris extent and thickness data

We used globally distributed debris thickness map developed by

Rounce et al. (2021) which was derived via sub-debris melt inversion method followed by a surface temperature inversion approach to estimate the distributed debris thickness over the glacier's entire debris-covered area.

4. Methodology

4.1. Glacier mapping

The RGI V6.0 (Pfeffer et al., 2014) glacier outlines were manually adjusted using the orthorectified images from the corresponding years. We manually adjusted glacier extents using surface slope, curvature and shaded relief generated from the corresponding DEMs (Bolch et al., 2007). Subsequent adjustments were carried out for the other available time periods by taking advantage of the corresponding ortho images and DEMs. We classified the glaciers as clean or debris-cover according to the globally distributed debris thickness map given by Rounce et al. (2021).

4.2. Glacier mass balance

4.2.1. DEM generation from stereo images

We generated DEM (30 m spatial resolution) from Hexagon KH-9 Mapping Camera (MC) imagery in Leica Photogrammetry Suite (LPS) by using a frame camera model with a focal length of 305 mm and flying height of ~170 km (Pieczonka and Bolch, 2015; Bhattacharya et al., 2016). Brown's physical model (Brown, 1971) was used to compensate for unknown lens and film distortions. The original geometry of the Hexagon KH-9 films was reconstructed by assessing their reseau grid (Pieczonka and Bolch, 2015, Bhattacharya et al., 2016). Interior orientation (pixel co-ordinates of an image point with the corresponding coordinates in the camera reference frame) was estimated by bi-linear interpolation (Pieczonka et al., 2013). Additionally, a local adaptive filter and histogram equalization was used to enhance the contrast of image subsets before mosaicking. The external orientation (transformation from the image coordinate system to ground coordinate system) was estimated by using GCPs (~40 GCPs) with an RMS of triangulation of $\leq$ ~1 pixel, collected from terrain corrected Landsat images as horizontal reference and the SRTM-3 arc *sec* (90 m) DEM as a vertical reference, and automatically generated tie points.

AMES Stereo Pipeline (ASP, v3.1.0), developed by the National Aeronautics and Space Administration (NASA) and later adapted and modified by Shean et al. (2016) Was used to generate DEMs from ASTER Level-1A (30 m spatial resolution) & Pleiades 1B imagery (4 m spatial resolution). A void-filled SRTM-1 arc sec DEM was used for initial orthorectification; however, SRTM-3 arc sec DEM was used for DEM generation. A semi-global matching (SGM) correlation algorithm (Hirschmuller, 2007) with 7 × 7-pixel window size was used as suggested by Shean et al. (2020). To remove the artifacts in the disparity images we used ASP's default SGM disparity map filters. All valid pixels in the disparity image were adjusted based on the Bayes EM weighted affine adaptive window correlator (Nefian et al., 2009). A rational polynomial coefficient (RPC) model (Grodechi and Dial, 2003) was used in stereo triangulation for both ASTER L1A and Pleiades 1B data. Finally, the output DEMs were generated for ASTER L1A and Pleiades 1B respectively with WGS84 ellipsoidal datum.

For the calculation of the elevation differences of ICESat-2 data, we used all the points from the whole period of operation (2018–2023) and the SRTM-3 arc sec DEM as the reference surface. Using the time difference between the SRTM acquisition and each particular ICESat-2 points, we calculated the elevation difference averaged over the period (Supplementary Fig. 5).

4.2.2. DEM coregistration

Each DEM was co-registered with the void filled SRTM-1 arc sec DEM following the analytical approach developed by Nuth and Kääb (2011). Further, the tilt between two DEMs was estimated by applying a 2-D first order polynomial trend surface analysis (Pieczonka et al., 2013) relative to the SRTM-1 arc sec DEM, which minimized the elevation dependent biases. To eliminate small rotational effect, de-ramping was also used by estimating a 1-D polynomial over the entire DEM difference image (Pieczonka and Bolch, 2015).

4.2.3. Outlier removal, gap filling and mass balance derivation

For ASTER DEM differences, first, we removed all elevation differences outside ±150 m from the DEM difference images. Then, for each 100 m elevation bin, we excluded all differences outside $\mu \pm 3\sigma$ (μ and σ are the mean and standard deviation within the elevation bin) (Gardelle et al., 2013). For KH9 DEM differences, we followed the technique proposed by Pieczonka and Bolch (2015), and applied an elevation dependent sigmoid function to remove the outliers. The detailed methodology has been discussed in supplement (Supplementary Note 1).

All data gaps in the DEM difference images were filled in two steps to get continuous elevation change grids. To maintain a consistent elevation change, small data gaps (< 5 pixels) were filled in the first step by the mean elevation of the neighboring pixels (4 × 4 pixels windows). The larger data gaps, predominant in the accumulation regions, were filled by median hypsometric approach described by McNabb et al. (2019) at 100 m elevation bins.

4.2.4. Uncertainties estimation

We estimated uncertainties associated with glacier length fluctuations, glacier area changes and overall glacier mass balance. Detailed methodology of the uncertainty estimation has been discussed in supplement (Supplementary Note 2).

The glacier length change uncertainty was estimated by considering the spatial resolution of the associated images and the coregistration error between the images as described by Hall et al. (2003). The glacier area change uncertainty was estimated by considering the mapping inaccuracy during the adjustment of the glacier polygons. The overall uncertainty for the area change was estimated by the law of error propagation (Pieczonka and Bolch, 2015; Bhattacharya et al., 2016).

Overall glacier mass balance uncertainty was estimated by considering the uncertainty associated with (1) the surface elevation change (Rolstad et al., 2009; Fischer et al., 2015) (2) the glacier area/volume change (Brun et al., 2017) and (3) the volume to mass conversion by considering conversion factor of 0.85 ± 0.06 following Huss (2013). We also considered the uncertainty resulting from the inconsistency of the percentage of data gaps, which varies from 32.5% (1973–2006) to 16.1% (2000−2020), in elevation change images (Brun et al., 2017; Mukherjee et al., 2022).

4.2.5. ICESat-2 data processing

We selected ICESat-2 points on the glacier further than 20 m from its margine and <200 m above the reference DEM to filter out noisy points. HMA DEM from 2015 was used as the elevation reference to account to shifts between the repeated tracks following (Kropáček et al., 2014; Shen et al., 2022). In the next step we calculated median and standard deviation of elevation difference for each track. Only tracks with >10 points in the glacier extent were used in the further analysis. To better understand the kinematics of the glacier during the surge, we separated the points into elevation zones.

5. Results

5.1. Multi-temporal glacier area changes

We investigated (~445 glaciers) glacierized area of 812.5 ± 23.6 km^2 in 1973, which decreased to 758.8 ± 22.7 km^2 in 2020, hence the area reduced by 53.7 ± 1.4 km^2 over the entire observation period (1973–2020). The mean glacier area lost during 2000–2020 was slightly higher (1.34 ± 0.07 km^2 a^{-1}) as compared to previous time span (1.01

± 0.05 km^2 a^{-1}) of 1973–2000. Only 7% of the investigated glaciers (1973) had an area extent of >5 km^2, which constituted ~66% (535.1 ± 27.8 km^2) of glacierized area. Whereas, ~44% of the glaciers with an area of <0.25 km^2, covers only ~3.0% (23.6 ± 1.8 km^2) glacierized area.

Overall, debris-covered glaciers (Rounce et al., 2021) occupied an area of 685.6 ± 13.1 km^2 (~84.4%) during 1973, with ~264 clean-ice glaciers constituting the remaining ~15.6% of the overall glacier area (126.9 ± 10.5 km^2). During the entire observation period (1973–2020), debris-covered glaciers lost less glacierized area (0.07 ± 0.01% a^{-1} or 0.49 ± 0.03 km^2 a^{-1}) compared to their counterpart (0.5 ± 0.03% a^{-1} or 0.65 ± 0.04 km^{2}a^{-1}). The detailed description of the glacier area change in different time scale are provided in Supplementary Table 2.

5.2. Multi-temporal glacier mass balance estimates

Glaciers in the study region experienced considerable downwasting (Fig. 2) during the observation period (1973–2020) with an average thickness loss of 18.7 ± 2.52 m corresponding to a mean mass loss of 0.34 ± 0.09 m w.e. a^{-1} (Table 1).

The rate of glacier mass loss in the region slightly decreased between 2000 and 2006 (−0.22 ± 0.10 m w.e. a^{-1}) compared to the previous time span (1973–2000: −0.30 ± 0.12 m w.e. a^{-1}). However, mass loss rates in the most recent period (2015–2020) appear to have increased significantly (−0.68 ± 0.09 m w.e. a^{-1}) compared to that of the 2006–2015, which was −0.37 ± 0.14 m w.e. a^{-1}, and to the total mean mass loss (0.40 ± 0.09 m w.e. a^{-1}) over the whole observation period (1973–2020),

Overall, the debris-covered glaciers lost slightly more ice (−0.37 ± 0.10 m w.e. a^{-1}) as compared to clean-ice glaciers (−0.28 ± 0.10 m w.e. a^{-1}) during the entire observation period (1973–2020). Both clean-ice (−0.54 ± 0.12 m w.e. a^{-1}) and debris-covered (−0.76 ± 0.11 m w.e. a^{-1}) glaciers experienced an accelerated mass loss in the most recent time period (2015–2020), but the rate of acceleration was different (debris covered: 51% and clean ice: 43%) as compared to the previous time period (2006–2015). Although the debris-covered glaciers exhibited only slightly higher mass loss in our study area, but the glacier parts covered with debris (Rounce et al., 2021) showed significantly exacerbated surface lowering (−0.62 ± 0.14 m a^{-1} during 1973–2000 and −

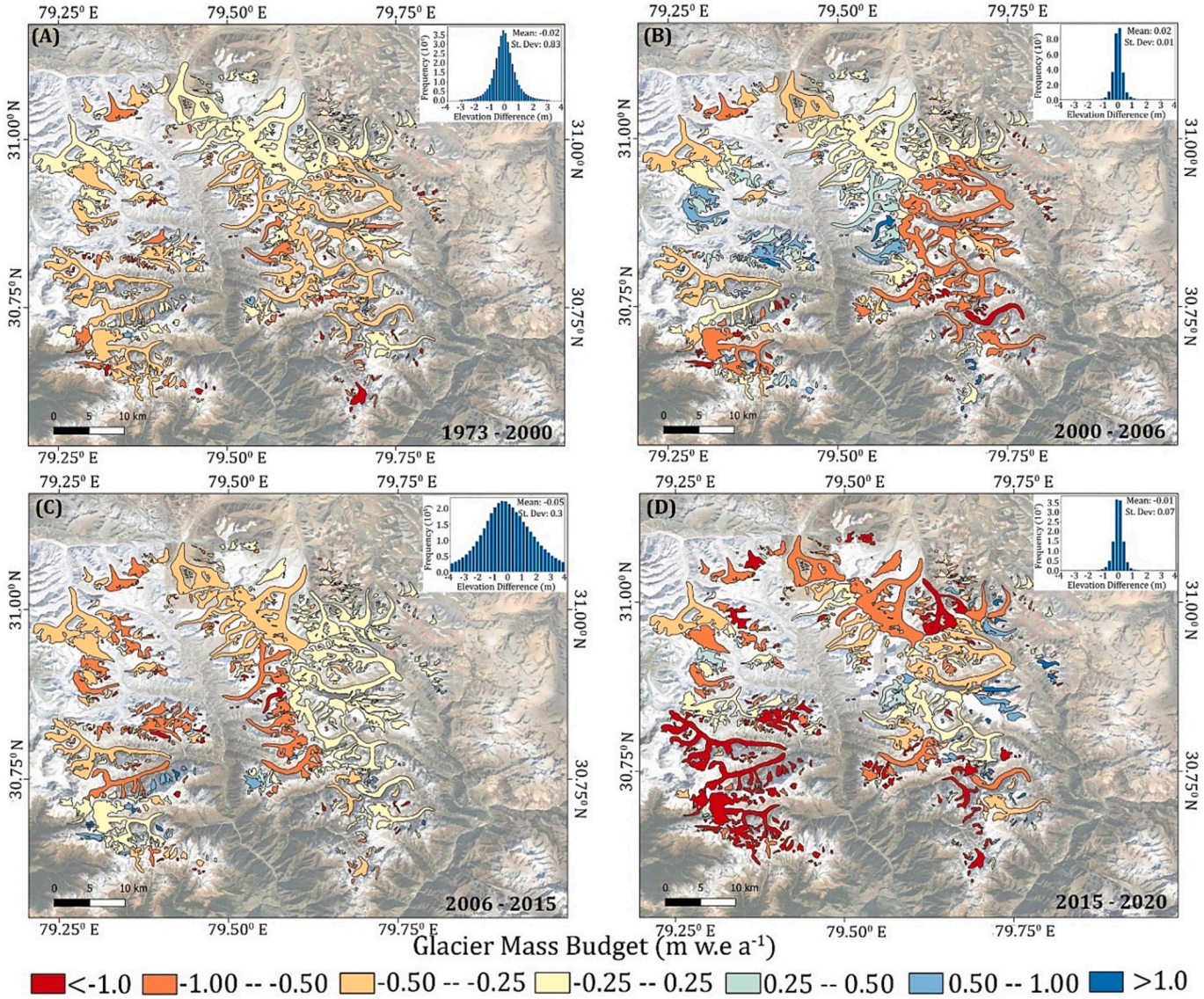

Fig. 2. Multi-temporal glacier mass budget of the study region for the periods of (A) 1973–2000; (B) 2000–2006; (C) 2006–2015 and (D) 2015–2020. The color coding represents mean mass balance. The off-glacier statistics are also shown (inset). The background image is Google Satellite Image' available in QGIS Quick Map Services plugin.

Table 1
Elevation changes and geodetic mass balance estimates of glaciers across the study region and the Alaknanda Basin in different time periods (Bold represents overall study period).

Time periods	Overall study area						
	Valid data (%)	Overall glaciers (445)		Debris-covered glaciers (181)		Clean-ice glaciers (264)	
		Elevation change (m)	Mass balance (m.w.e. a^{-1})	Elevation change (m)	Mass balance (m.w.e. a^{-1})	Elevation change (m)	Mass balance (m.w.e. a^{-1})
1973–2000	68.2	−9.45 ± 2.24	−0.30 ± 0.12	−10.3 ± 2.95	−0.32 ± 0.14	−7.83 ± 2.95	−0.25 ± 0.14
2000–2006	71.4	−1.56 ± 0.72	−0.22 ± 0.10	−1.62 ± 0.84	−0.23 ± 0.11	−1.20 ± 0.88	−0.17 ± 0.11
2006–2015	75.6	−3.95 ± 0.88	−0.37 ± 0.14	−3.96 ± 0.91	−0.37 ± 0.14	−3.24 ± 0.97	−0.31 ± 0.15
2015–2020	76.5	−4.00 ± 0.59	−0.68 ± 0.09	−4.45 ± 0.75	−0.76 ± 0.11	−3.20 ± 0.85	−0.54 ± 0.12
2000–2020	83.9	−10.2 ± 1.53	−0.43 ± 0.06	−10.4 ± 1.92	−0.44 ± 0.09	−8.96 ± 1.92	−0.38 ± 0.10
1973–2006	67.5	−11.1 ± 1.51	−0.29 ± 0.07	−12.1 ± 1.85	−0.31 ± 0.09	−9.11 ± 1.76	−0.23 ± 0.10
1973–2015	69.3	−15.5 ± 1.75	−0.31 ± 0.06	−16.5 ± 2.55	−0.33 ± 0.09	−11.0 ± 2.35	−0.22 ± 0.09
2000–2015	79.1	−5.72 ± 0.78	−0.32 ± 0.08	−5.98 ± 1.08	−0.34 ± 0.10	−5.24 ± 1.18	−0.30 ± 0.10
2006–2020	72.4	−8.28 ± 0.68	−0.50 ± 0.07	−8.78 ± 0.98	−0.53 ± 0.09	−6.82 ± 0.88	−0.41 ± 0.09
1973–2020	**69.3**	**−18.7 ± 2.52**	**−0.34 ± 0.09**	**−20.3 ± 3.14**	**−0.37 ± 0.10**	**−15.5 ± 3.17**	**−0.28 ± 0.10**

Time periods	Alaknanda Basin						
	Valid data (%)	Overall glaciers (246)		Debris-covered glaciers (132)		Clean-ice glaciers (114)	
		Elevation change (m)	Mass balance (m.w.e. a^{-1})	Elevation change (m)	Mass balance (m.w.e. a^{-1})	Elevation change (m)	Mass balance (m.w.e. a^{-1})
1973–2000	68.7	−11.3 ± 2.98	−0.36 ± 0.09	−11.9 ± 3.13	−0.37 ± 0.10	−7.29 ± 2.93	−0.23 ± 0.09
2000–2006	76.1	−1.56 ± 0.85	−0.22 ± 0.11	−1.66 ± 0.78	−0.24 ± 0.13	−1.36 ± 0.69	−0.19 ± 0.12
2006–2015	77.6	−4.59 ± 1.02	−0.43 ± 0.13	−5.22 ± 0.85	−0.49 ± 0.15	−3.87 ± 0.81	−0.37 ± 0.14
2015–2020	81.8	−4.75 ± 1.08	−0.81 ± 0.14	−4.65 ± 0.81	−0.79 ± 0.14	−4.10 ± 0.78	−0.70 ± 0.13
2000–2020	87.8	−10.2 ± 2.43	−0.43 ± 0.10	−10.2 ± 2.91	−0.43 ± 0.12	−9.31 ± 2.32	−0.35 ± 0.10
1973–2006	69.7	−12.2 ± 2.10	−0.31 ± 0.12	−13.1 ± 2.15	−0.34 ± 0.14	−7.98 ± 1.59	−0.21 ± 0.12
1973–2015	70.1	−16.6 ± 2.48	−0.34 ± 0.12	−16.6 ± 4.65	−0.34 ± 0.10	−11.4 ± 4.25	−0.23 ± 0.09
2000–2015	80.2	−5.75 ± 1.05	−0.33 ± 0.10	−6.15 ± 1.65	−0.35 ± 0.10	−4.98 ± 1.51	−0.28 ± 0.11
2006–2020	74.6	−10.2 ± 1.95	−0.62 ± 0.08	−11.0 ± 1.88	−0.67 ± 0.12	−8.43 ± 1.78	−0.51 ± 0.11
1973–2020	71.4	**−21.9 ± 4.95**	**−0.40 ± 0.09**	**−22.1 ± 5.12**	**−0.40 ± 0.09**	**−16.9 ± 4.92**	**−0.31 ± 0.09**

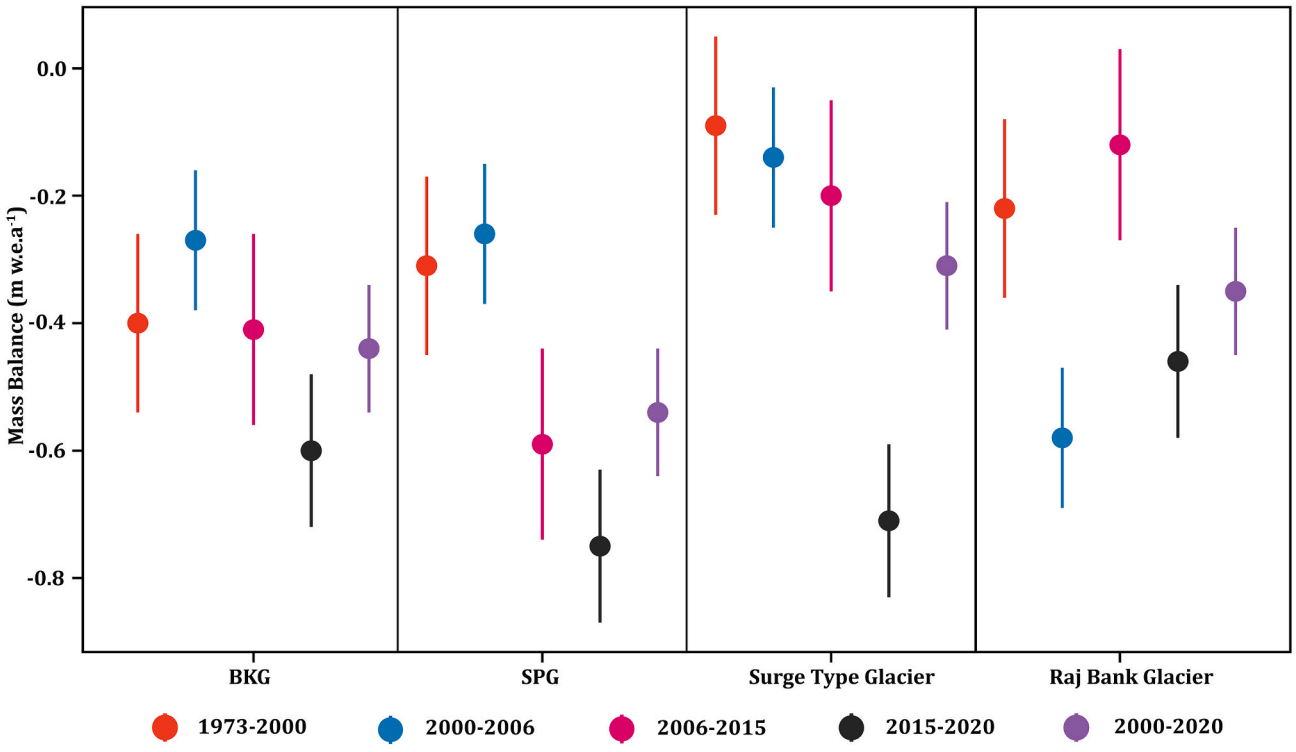

Fig. 3. Multi-temporal glacier mass balance of the Bhagirath Kharak (BKG), Satopanth (SPG), Surge-type (RGI60–14.26971) and Raj Bank (RGI60–15.06559) glaciers (Fig. 1).

0.95 ± 0.13 m a^{-1} during 2000–2020).

In addition to the region wise results, multi-temporal mass balance of four individual glaciers (Fig. 3) with variable debris cover, with percentages ranging from 58.6% to 3.0% (Rounce et al., 2021), were investigated more closely. The behaviour of two of the region's largest glaciers (Fig. 1), the Bhagirath Kharak (BKG, Glacier 3) and the Satopanth (SPG, Glacier 4) from where the Alaknanda River originates, followed the regional trend in glacier mass change. The mass loss of SPG (58.6% debris cover) and BKG (37.5% debris cover) were estimated as −0.31 ± 0.14 m w.e. a^{-1}, and − 0.40 ± 0.14 m w.e. a^{-1} respectively during 1973–2000, which increased to −0.44 ± 0.10 m w.e. a^{-1}, and − 0.54 ± 0.10 m w.e. a^{-1} respectively during 2000–2020. Another comparatively less debris-covered (3.0% of its total surface) glacier (Glacier −1 in Fig. 1; RGI60–14.26971), flowing towards the Tibetan plateau, exhibited contrasting behaviour in its mass budget. The glacier was nearly balanced between 1973 and 2000 (−0.09 ± 0.14 m w.e. a^{-1}) but it began losing mass after 2000 (−0.14 ± 0.11 m w.e. a^{-1} during 2000–2006) and reached its maximum (−0.71 ± 0.12 m w.e. a^{-1}) during the most recent time period (2015–2020) with an average mass loss of −0.31 ± 0.10 m w.e. a^{-1} between 2000 and 2020. Moreover, the Raj Bank Glacier (Glacier 2 in Fig. 1, RGI60–15.06559), located in the south eastern part of our study area, revealed a different pattern of multi-temporal mass budget, though exhibiting similar trend in glacier mass budget considering just two periods, one before and another after 2000 (−0.22 ± 0.14 m w.e. a^{-1} between 1973 and 2000 and 0.35 ± 0.10 m w.e. a^{-1} between 2000 and 2020).

In addition to the four periods (1973–2000, 2000–2006, 2006–2015, 2015–2020) mentioned above, we also calculated the mass balance using all possible combinations of the DEMs generated in this study. This leads to ten different mass balance measurements (Table 1).

5.3. Meteorological conditions and climate variability of the study area

5.3.1. ERA5 land summer and annual temperature

We observed maximum summer temperature (July-Aug-Sept) of ~5.3 °C in 2020, which was ~1.4 °C above the overall (1973–2020) average summer temperature (~3.9 °C) from ERA5 Land reanalysis data, In the last mass balance period (2015–2020), the summer temperature (~4.3 °C) was substantially higher (~0.5 °C) than during the first mass balance period (1973–2000) (~3.8 °C), leading to a positive summer temperature anomaly (difference from mean summer temperature of the whole period) during 2015–2020 (Fig. 4A). Moreover, during 2000–2006, when we measured low mass loss, average summer temperature slightly decreased (by ~0.1 °C) compared to the preceding time period (1973–2000). Additionally, annual mean temperature (−5.1 °C) also increased by ~0.6 °C during 2015–2020 as compared to the previous time period of 1973–2000 (−5.7 °C).

5.3.2. ERA5-Land solid and liquid precipitation

Maximum solid precipitation (snow fall ~1564 mm) occurred in 1975, ~49% more than the average (~1047 mm) for the entire period (1973–2020). However in 2020, the yearly average snowfall decreased by ~113 mm compared to the mean overall (1973–2020) snowfall. The winter precipitation (Dec-Jan-Feb-March) also demonstrated a declining trend throughout the course of the observation period. Winter precipitation dropped after 2000 (2000–2020) by ~120 mm (~11.6%) compared to 1973–2000, moreover, a significant decline was observed (~149 mm or ~ 14.4%) in the most recent observation period (2015–2020). Similar to winter precipitation, annual precipitation also exhibited a declining trend throughout the observation period over the study area. When compared to the period prior to 2000, annual precipitation reduced by ~10.6% between 2000 and 2020.

5.3.3. Weather station-based temperature and precipitation

We also investigated the temperature and precipitation data of the Mukhim weather station (Fig. 4A & 4B). The summer temperature of Mukhim station increased by ~0.8 °C between 2000 and 2007 when compared to the period before 2000 (1973–2000). A significant increase of annual maximum temperature (~1.0 °C) during 2000–2007 was observed, however, annual minimum temperature slightly decreased (~0.2 °C) during the same period. An increase of ~300 mm (~16%) annual precipitation was observed after 2000 (2000–2007) when compared to the earlier time period (1973–2000). However, a minor decrease (~2%) in winter precipitation was observed during 2000–2007.

5.3.4. Comparison of ERA5 Land and weather station data

Though both the datasets (ERA5 Land grided and station data) showed similar trend during our observation period, direct comparison of station data with reanalysis data is biased because it is only a point measurement and the station is situated at a much lower elevation (~1981 m a.s.l) as compared to the mean elevation (~5478 m) of the study area. Therefore, we compared ERA5 reanalysis data of the grids containing the Mukhim weather station (Supplementary Table 3). Summer, winter and annual temperature exhibited a higher correlation which varies from $r = 0.52$ and $p = 0.001$ (summer temperature) to $r = 0.65$ and $p = 0.0002$ (winter temperature). Although annual precipitation ($r = 0.22$, $p = 0.18$) did not show any significant correlation, but winter precipitation showed a significant correlation ($r = 0.61$, $p = 0.0001$) between the datasets (Supplementary Table 3). Based on significant correlation of ERA5 Land with station data, we consider ERA5 Land data to be a good representation of the climate over glaciated

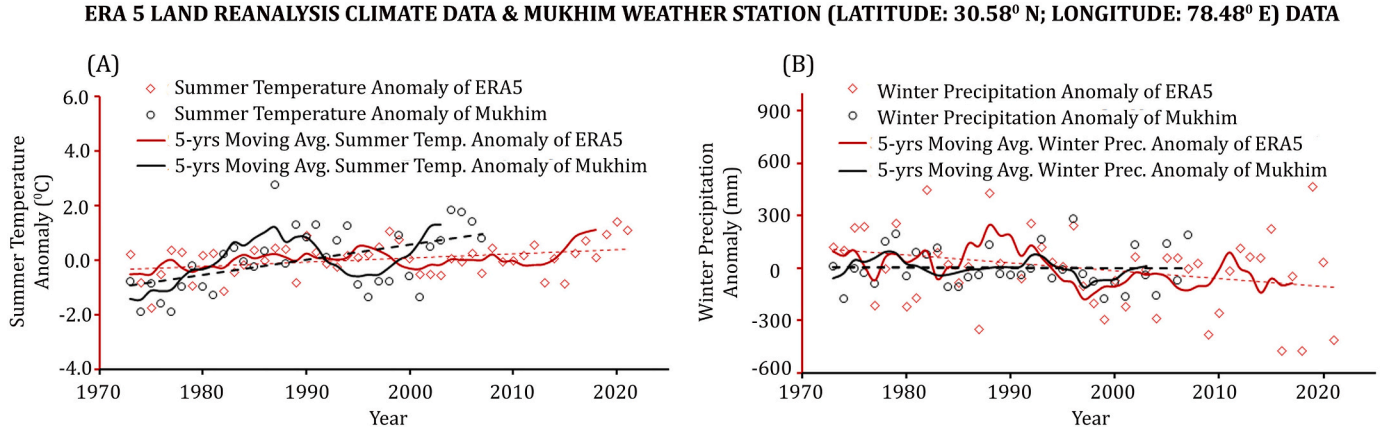

Fig. 4. Comparison of (A) Summer temperature and (B) winter precipitation anomaly with 5-years moving average derived from ERA5 Land reanalysis and Mukhim weather station data.

regions.

5.4. Variations of non-climatic attributes of the study area

We estimated different individual glacier specific attributes such as glacier morphometry (slope, aspect, median elevation and glacier area), glacier dynamics and debris thickness in our study region.

5.4.1. Glacier median elevation

It has been observed that the balanced-budget equilibrium-line altitude (ELA) significantly correlated with median elevation (Braithwaite, 2009), and therefore, median glacier elevation can act as a proxy of ELA (Braithwaite and Raper, 2009). On the other hand, ELA and glacier mass balance are strongly correlated (Braithwaite, 2009). We found that the minimum and maximum elevation of the investigated glaciers in our study region were 3750 m and 7454 m respectively, with a median elevation ranging from 4324 m to 6874 m. Median elevation of only 20% ($n = 88$) of the glaciers in our sample were above the average median elevation (5300 m) of the study area.

5.4.2. Glacier aspect

Out of the 445 glaciers, we found that 207 glaciers are flowing in an approximately northerly direction (NW, N, & NE), whereas only 36 and 55 glaciers, respectively, are flowing towards the west and east and remaining 147 glaciers are flowing in southern (SE, S and SW) direction. We also estimated that the northern aspect (~47%) glaciers constituted ~48% glacier area, whereas, ~33% of glaciers were flowing towards the south (SE, S & SW) of the study region and occupied only ~18% of the overall glacier area (Supplementary Fig. 1).

5.4.3. Glacier slope

Another important factor that has a substantial impact on the glacier-specific mass budget is glacier slope. Knowing the average slope of the glaciers is important as a steeper overall slope indicates a higher ice dynamic, which plays a significant role to control glacier flow and in turn glacier mass turnover. We found the mean slope of all investigated glaciers was 25.4° with minimum and maximum slope varied from 5.0° to 53.1° respectively. Additionally, we also found that the majority of the glacier area (719.1 km^2 or 91.5%) has a slope lower than the average slope of all the glaciers (25.4°) and remaining 66.5 km^2 glacier area has a slope higher than the average slope of the glaciers in the study region.

5.4.4. Glacier dynamics

We observed a constant decrease of annual surface velocity across the entire study region irrespective of their surface characteristics (Fig. 5). The mean annual velocity for all the glaciers decreased from 5.9 ± 2.1 ma^{-1} in 2000 to 3.6 ± 1.9 ma^{-1} (21.5 ± 6.3% dec^{-1}) in 2018. Glacier surface velocity of the debris covered and clean ice region were also reduced by 22.8 ± 3.1% dec^{-1} and 21.1 ± 5.1% dec^{-1} respectively during the same time period. The average velocity of the clean ice glaciers (5.1 ± 1.8 m a^{-1}) were slightly higher than the mean velocity of the region (4.9 ± 1.9 m a^{-1}), whereas, debris cover (4.5 ± 2.0 m a^{-1}) showed less velocity than the mean during 2000–2018, though the differences are not statistically significant. However, Fig. 5B clearly indicates that on an average, debris covered glaciers are slower than clean ice glaciers.

5.4.5. Debris thickness

According to the globally distributed debris thickness map (Rounce et al., 2021) of all investigated glaciers, about 41% of glaciers were found to be covered with debris, with the amount of debris varying from 0.76% (RGI15.0713) to 67% (RGI14.27012) of the glacier area. The absolute debris covered area varied from 0.02 km^2 (RGI15.07122) to 22.5 km^2 (RGI15.07303). The glacier wise average debris thickness varied from ~0.009 m to ~2.15 m with an average of ~0.29 m (Rounce et al., 2021) during 2000 in the study region.

6. Discussion

6.1. Comparison of glacier area and mass change variability with other published studies

Despite the fact that the Indian Himalayan region's glaciers have been extensively studied over the past few decades, the majority of these studies have been either limited in time scale, focusing on only one or two time periods (Bhambri et al., 2011; Bandyopadhyay et al., 2019; Remya et al., 2020, 2022; Mishra et al., 2022; Bhambri et al., 2023), or in their spatial extent, focusing on a small number of glaciers (Gautam and Mukherjee, 1992, Dobhal et al., 2008, 2013; Bhattacharya et al., 2016; Kumar et al., 2017a, 2017b; Shah et al., 2019 etc.). Our results offer a regional, long-term perspective on glacier change, which are derived from nearly five decades of remotely sensed data.

A recent study (Mishra et al., 2022) reported that the total glacierized area (~175 glaciers) in the upper Alaknanda Basin reduced by between 0.13 ± 0.1% a^{-1} (1994–2000) to 0.15 ± 0.3% a^{-1} (2000–2020). Our estimated results for a slightly larger population of glaciers (~246 glaciers) in the Alaknanda Basin also demonstrated similar area reduction rate of 0.12 ± 0.1% a^{-1} (1973–2000) to 0.16 ± 0.1% a^{-1} (2000–2020) with an average of 0.13 ± 0.1% a^{-1} (1973–2020). While Bhambri et al. (2011) reported a 0.48 ± 0.2 km^2

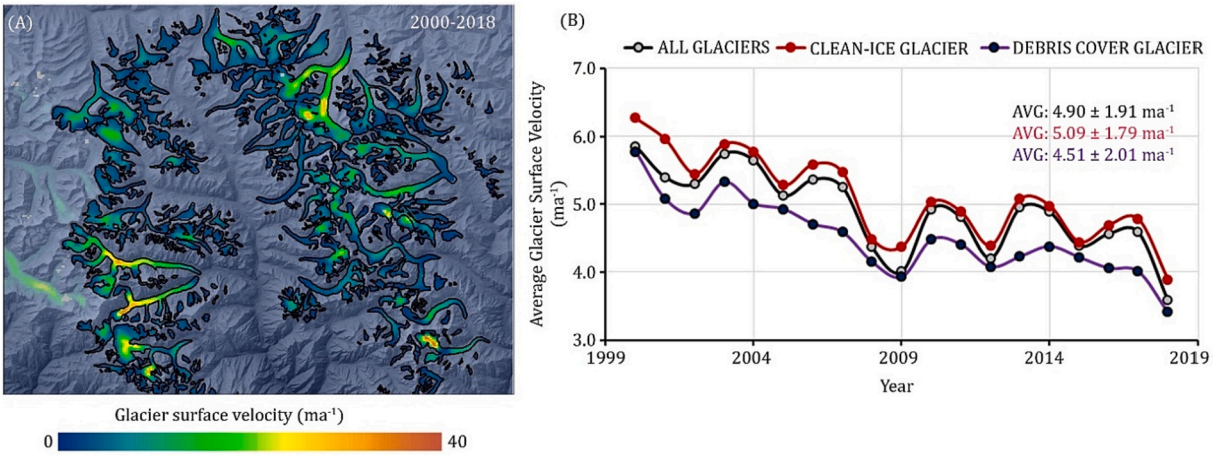

Fig. 5. (A) Average annual ITS_LIVE derived velocity field from 2000 to 2018 of the study area and (B) average velocity of all the investigated glaciers, clean ice glaciers and debris cover glaciers.

a^{-1} reduction of the glacierized area in the Saraswati/Alaknanda basin (~83 glaciers) from 1968 to 2006, we found higher overall recession rate (1.09 ± 0.2 km^2 a^{-1}) for ~445 glaciers between 1973 and 2006, likely as a result of the different glacier populations and time periods taken into account.

We also found that the overall estimated glacier mass balance of this study is generally consistent with other global (Brun et al., 2017; Hugonnet et al., 2021) and regional studies (Bandyopadhyay et al., 2019; Remya et al., 2020, 2022), despite the use of various datasets and methodologies. Our mass loss estimate (−0.32 ± 0.08 m w.e. a^{-1}) during 2000–2015 was slightly lower as compared to Brun et al. (2017) (−0.35 ± 0.10 m w.e. a^{-1} from 2000 to 2016), however within the uncertainty limit. Additionally, our mass balance estimate between 2000 and 2020 (−0.43 ± 0.06 m w.e. a^{-1}) was slightly lower when compared with another global mass balance study (Fig. 6; Hugonnet et al., 2021) during the same time span (−0.37 ± 0.06 m w.e. a^{-1}). Our results over the 2000–2015 period (−0.33 ± 0.09 m w.e. a^{-1}) are also in line with those of Bandyopadhyay et al. (2019) (2000–2014; −0.32 ± 0.05 m w.e. a^{-1}). Our estimates of glacier mass loss for entire study region during 2000–2020 are greater (−0.43 ± 0.06 m w.e. a^1) than those of Remya et al., (2020, 2022) (−0.28 ± 0.08 m w.e. a^{-1}) during 2000–2017. Differences between our results and those of Remya et al., (2020, 2022) may be due to their small number of investigated glaciers (61), or the complex penetration bias of the SRTM DEM, which may result in an underestimation of glacial surface elevation change rates by up to 20% (Vijay and Braun, 2016; Mukherjee et al., 2018).

A few studies estimated glacier scale mass balance along the Garhwal Himalayan region using different techniques, datasets and time scales (Supplementary Table 4). Glaciological mass balance was estimated for the four glaciers, Dokriani (7 km^2), Chorabari (6.7 km^2), Tipra Bank (7 km^2) and Dunagiri (2.6 km^2), in the Garhwal Himalaya at different time periods. All four glaciers are losing mass continuously. However, the mass loss rate is heterogeneous in temporal scale. Among those, Tipra Bank Glacier experienced much less ice mass loss (−0.14 m w.e. a^{-1}) during 1981–1988 and small Dunagiri Glacier showed considerably more mass loss (−1.04 m w.e. a^{-1}) during 1984–1990. Such excessive mass loss is probably due to the presence of steep headwall which might cause frequent ice loss through avalanches (Azam et al., 2018). Moreover, rapid glacier wasting suggests the strong vulnerability of small glaciers compared to their larger counterparts (Paul et al., 2004). The geodetic estimates of the Gangotri Glacier (~ 30 km), in the vicinity of our study region, also showed considerable mass loss (−0.29 ± 0.12 m w.e. a^{-1} by Bhattacharya et al., 2016) in recent period (2006–2014). Mass loss using Synthetic Aperture Radar (SAR) based DEMs showed even a more negative mass budget (−0.55 ± 0.42 m w.e. a^{-1} by Bhushan et al., 2018 and − 0.55 ± 0.03 m w.e. a^{-1} by Bandyopadhyay et al., 2019) for this glacier after 2000. A possible explanation for the deviations could be the influence of different data sources, especially complicated penetration biases of the SAR-based DEMs. Similar strong mass loss in recent time was also reported for Bhagirath Kharak and Satopanth glaciers by Brun et al. (2017), Hugonnet et al. (2021) and Remya et al. (2022), which was also comparable with our estimate during 2000–2020 (Supplementary Table 4).

The multi-temporal global glacier elevation change grid produced by Hugonnet et al., 2021 is in tendency in line with our regional estimate, but we found differences in short-term heterogeneous variations, such as glacier surge and dynamic separation of glaciers. For instance, during 2000–2020 we found comparable mass balance of −0.31 ± 0.10 m w.e. a^{-1} with Hugonnet et al. (2021) (−0.25 ± 0.05 m w.e. a^{-1}) for the Glacier 1 (in Fig. 1; RGI60–14.26971), however, our mass balance during 2015–2020 showed that the glacier lost significant ice (−0.71 ± 0.12 m w.e. a^{-1}) due to the massive surge event, which was significantly different (−0.10 ± 0.05 m w.e. a^{-1}) from Hugonnet et al. (2021). This exemplifies that the statistical averaging of all available elevation change grids during the entire time span (2015–2020) may obscure the rapid thinning in higher elevation over a short time span. Additionally, temporal adjustment of the original RGI glacier polygons is also important for accurate mass balance calculations, which was omitted in this global mass balance datasets.

The above results in general agree that glaciers in the region are continuously losing their mass and collectively show that mass loss accelerated in recent decades. In addition, we also observed that though debris-covered glaciers lost less area compared to the clean-ice glaciers, they are losing a greater mass of ice compared to clean ice-glaciers. A combination of multi-temporal mapping and mass budget calculations are essential to provide the best estimates of glacier wastage with time.

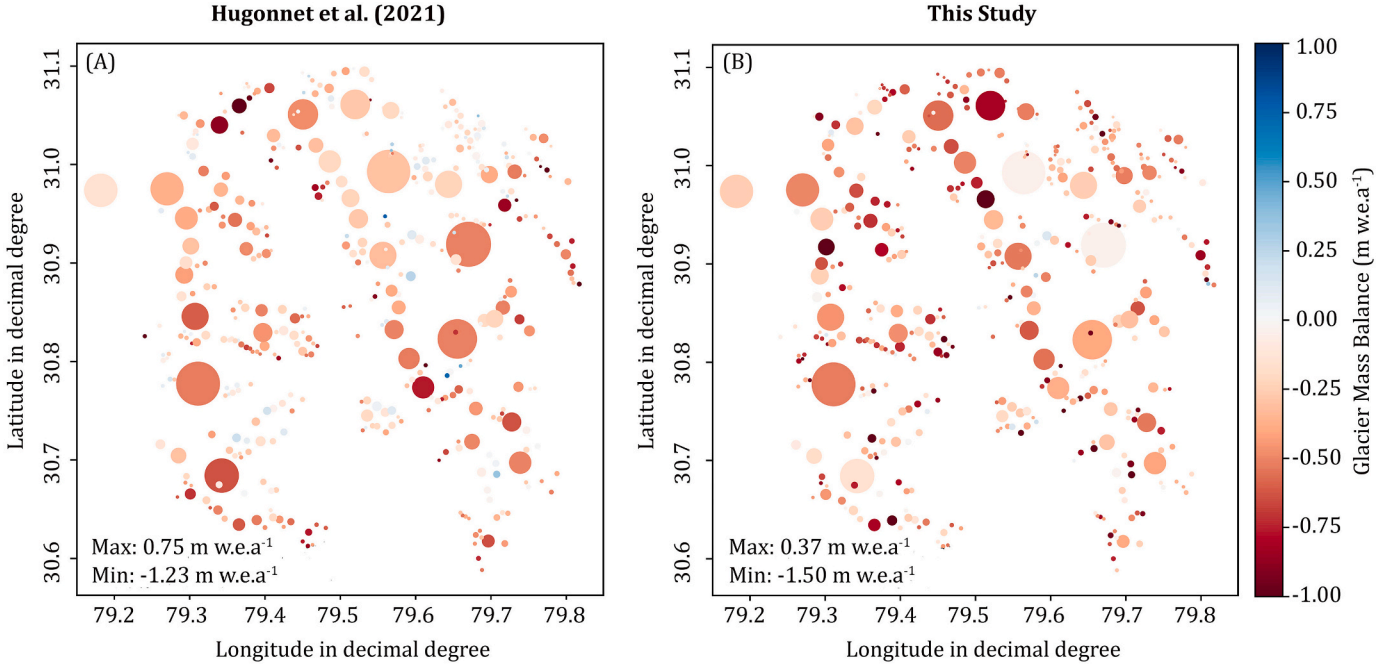

Fig. 6. Mass balance comparison of all the glaciers in this study with Hugonnet et al. (2021) for the year 2000–2020.

6.2. Glacier response to climate change

Glaciers in Garhwal Himalayan region are mainly influenced by the summer monsoon and winter snowfall (Thayyen and Gergan, 2010). During the observation period (1973–2020), ERA5-Land data showed that though the majority of average snowfall (~55.9% or 586 mm) occurred in winter (DJFM), ~22.3% (~234 mm) occurred in Spring (AMJ) and ~ 14.4% (~150 mm) in summer (JAS). Our analyses of meteorological station data and ERA5 Land climate reanalyses data suggest substantial changes in meteorological conditions in and around the Alaknanda basin which are closely linked to regional glacier mass balance. Several studies reported a significant increase in annual temperature (~0.1 °C to ~1 °C during 1866–2010) and corresponding decrease in annual precipitation in the broader Himalayan region (Basistha et al., 2009; Bhutiyani et al., 2010; Shrestha and Aryal, 2011; Singh et al., 2013). However, decadal scale variability using Climate Research Unit (CRU) data (Mishra et al., 2022) highlighted a considerable increase in annual precipitation after 2000.

We also analyzed temperature and precipitation and their anomalies (Fig. 7) derived from ERA5 Land reanalysis data over the same periods covered by geodetic mass balance estimates and observed a gradual increase in summer (0.6 °C) and annual (0.3 °C) temperature after 2000. However, solid and annual precipitation didn't show any significant trend during the entire observation period.

6.2.1. Analysis of climate drivers governing mass balance

We analyzed four climatic drivers: mean summer temperature, mean winter precipitation, mean annual temperature and mean annual snowfall (Fig. 8) across the ten mass balance periods (Table 1) to identify the most important climatic factors and their influence on glacier mass balance. We observe that summer temperature has the most significant control ($r = -0.97$, $p = 0$), followed by annual temperature ($r = -0.91$, $p = 0.002$), and winter precipitation ($r = 0.64$, $p = 0.04$). Annual snowfall does not have any significant correlation and does not play a noteworthy role to control the mass balance. Winter precipitation ($r = -0.64$, p = 0.04) and annual temperature ($r = 0.85$, p = 0.002) are highly correlated with summer temperature. The significant correlation of summer temperature with winter precipitation may be a result of increased water holding capacity of the warmer atmosphere according to Clausius-Clapeyron relation (Lenderink and van Meijgaard, 2008) resulting in increased precipitation. Considering these facts, we identify summer temperature as the most important factor controlling the mass balance in this region. Moreover, the relationship (Eq. Fig. 8A) indicates that the temperature sensitivity of the glaciers in this region is −0.6 m w. e. a^{-1} °C^{-1} and can be used as a metric to predict the mass balance for any intermediate year for this region. The model can also be used to forecast the mass balance for any future year, knowing the mean summer temperature. However, this model is built using the ERA5 Land climate data that is based on numerical weather prediction models and has its own uncertainties. In addition, if this model is implemented to predict mass balance using temperature values from other climate projection datasets, the bias between the two datasets must be investigated and eliminated.

6.2.2. Seasonal trends in temperature and precipitation

To investigate the impact of warming on the seasonal regime of ablation and accumulation, we examined the distribution of changes in temperature and precipitation in the study region (Fig. 9). ERA5 Land reanalysis data suggests an overall increase of Autumn (Oct-Nov) (~0.96 °C) and winter (Dec-March) (~0.52 °C) temperature in the most recent period (2015–2020) as compared to the first period (1973–2000). Similar temperature increase phenomenon (~0.41 °C) is also evident in between Summer-Autumn transition time (Sept-Oct) in the most recent period (2015–2020) as compared to the first period (1973–2000). Additionally, average summer (July-Sept) temperature also increased (~0.5 °C) in latest period (2015–2020).

The overall increase of autumn and summer temperature in the most recent period might have prolonged summer ablation in this region. Moreover, the annual and winter solid precipitation decreased by ~13.1% & ~9.8% respectively in recent period (2015–2020) compared to first mass balance period (1973–2000). Solid precipitation in spring season (Apr-June) also reduced by ~28.6% in 2015–2020 as compared to 1973–2000 which indicates a decreased accumulation in this region, which reduces the overall glacier volume and hence the ice velocity and mass turnover from higher to lower elevations.

6.2.3. Validation of ERA5 Land data with weather station data

To analyze the trend over the observation period between different climatic drivers we performed Mann–Kendall trend test, for both reanalysis and Mukhim station data (Supplementary Table 5) and found a general agreement between the reanalysis and weather station data. Significantly increasing trends for summer (Z = 2.04 and $p = 0.007$) and annual (Z = 2.54 and $p = 0.005$) temperatures were observed, while solid precipitation (Z = −1.50) decreased but not significantly ($p = 0.07$) throughout the observation period. Similar increasing trend of minimum annual temperature (AT_{Min}) was also observed for reanalysis and station data which was also reported by other studies in western Himalayan region (Shekhar et al., 2010; Bhambri et al., 2011). Similarly, maximum and minimum summer temperature (ST_{Max} & ST_{Min}) for both the datasets (ERA5 Land and station data) showed an increasing trend (Supplementary Table 5) throughout the observation period which was also evident in Bhambri et al. (2011). However, none of the

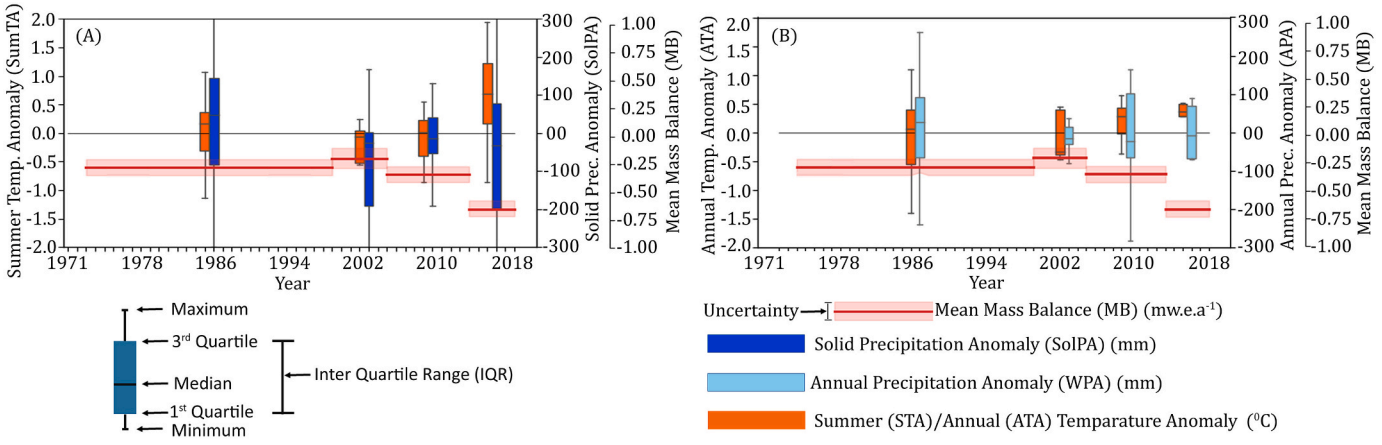

Fig. 7. Variations of different meteorological variables (A) summer temperature and solid precipitation anomaly, (B) summer temperature and annual precipitation anomaly and (c) summer temperature and winter precipitation anomaly with multi-temporal glacier mass balance.

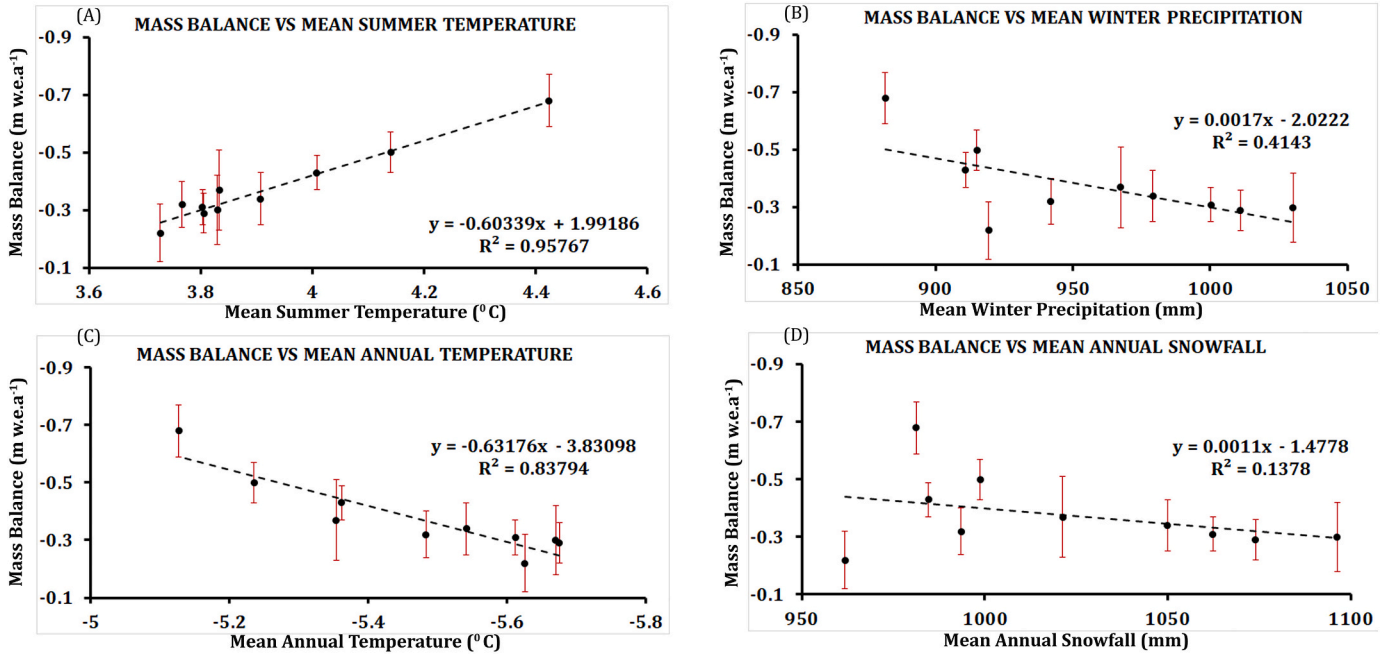

Fig. 8. Multi-temporal geodetic mass balance as a function of (A) summer temperature (B) winter precipitation (C) annual temperature and (D) annual snowfall.

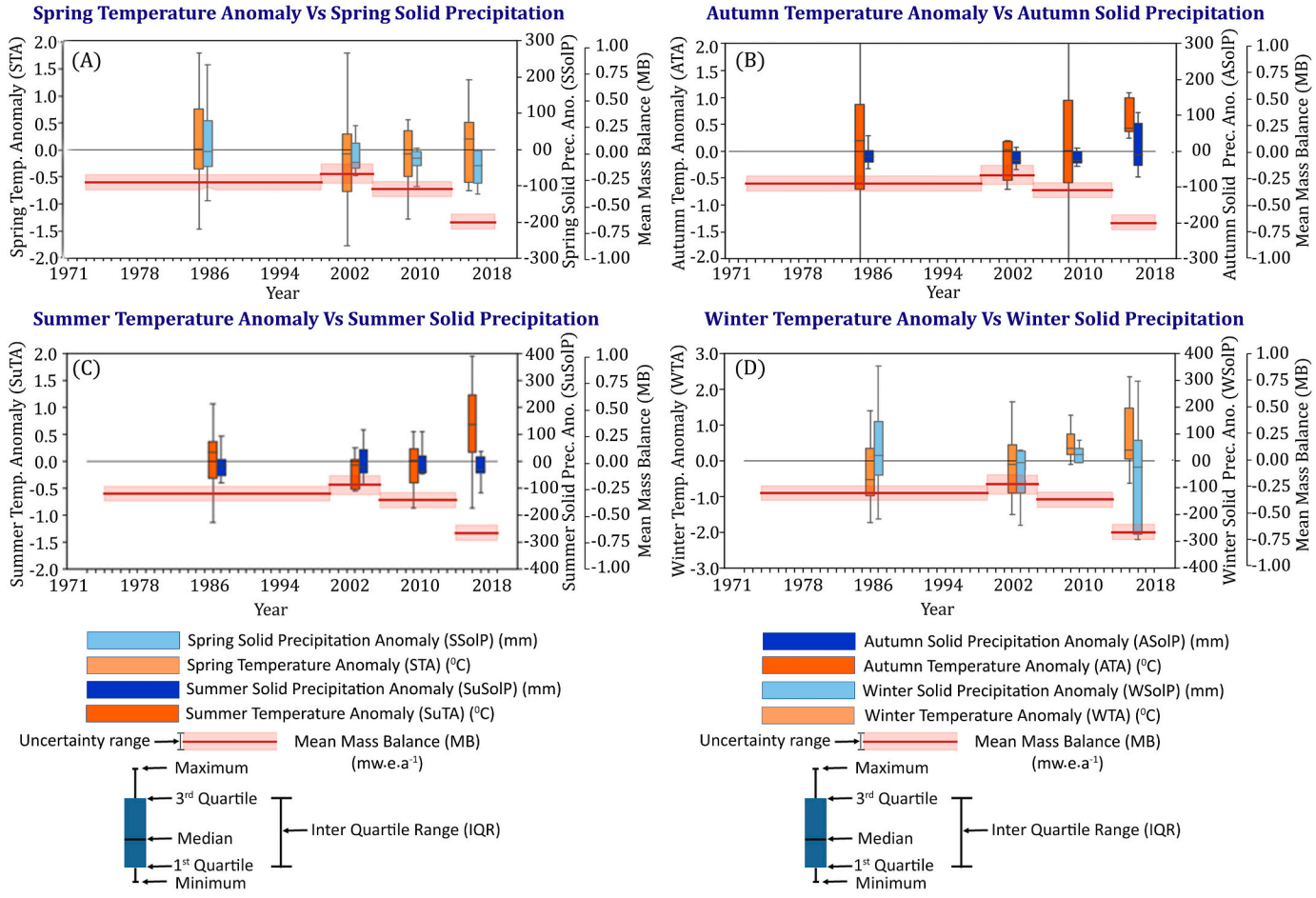

Fig. 9. Variation of seasonal temperature and solid precipitation anomaly with multi-temporal glacier mass budget.

precipitation components showed any significant trend during the observation period. Bhattacharya et al. (2021) stated that summer temperature was the most influencing factor to govern glacier mass balance in the recent decades in different climatic regions of High Mountain Asia (HMA), which is also evident from this analysis.

6.3. Implication of non-climatic attributes on glacier response

Glacier specific mass budget ranges from −1.2 m w.e. a^{-1} to +0.3 m w.e. a^{-1} throughout the full observation period. The heterogeneous glacier specific mass budget is often controlled by the individual glacier's attributes, such as, glacier morphometry, glacier ice dynamics and debris cover thickness and extent etc. (Vincent, 2002; Abermann et al., 2011; Huss, 2012; Davaze et al., 2020). Therefore, we investigated the effect of these factors on mass balance of the glaciers in our study region (Fig. 10, Fig. 11 & Supplementary Fig. 2 & 3).

6.3.1. Glecier morphometry

Numerous studies (Paul and Haeberli, 2008; Shukla and Qadir, 2016; Salerno et al., 2017; Brun et al., 2019; Bhattacharya et al., 2021) have suggested that various morphometric factors, such as topographic characteristics (i.e., glacier size, elevation, surface slope and aspect) (Berthier et al., 2007; Phan et al., 2014; Racoviteanu et al., 2014, 2015), ice surface dynamics (Bolch et al., 2011; Gardelle et al., 2013) debris cover (Scherler et al., 2011; Lejeune et al., 2013), and the presence of pro- and supraglacial lakes (Ragettli et al., 2016; King et al., 2019; Bhambri et al., 2023) influenced glacier mass balances on HMA region. However, regional variability of these factors are also evident. Overall, the regional-scale behaviour of glacier mass changes is influenced by multiple morphometric factors and is not still fully understood in our study region as multi-temporal observations are limited. Here we investigate different factors, such as elevation, slope, and aspect of the glaciers on glacier mass balance variability.

6.3.1.1. Glacier elevation and glacier area. The glacier elevation and hypsometry (distribution of glacier area at different elevations) are important factors controlling the mass balance. Elevation affects the primary climatic drivers, such as temperature and precipitation, which regulate the glaciers' mass balance. Similarly, glaciers with larger area coverage at higher elevations are likely to receive more accumulation, while glaciers with extensive coverage at lower elevations may experience higher ablation rates. Additionally, at various elevations, the seasons could also vary. For example, at the end of summer, snowfall may occur in the glaciers' upper accumulation regions, while melt continues close to the terminal (Cuffey and Paterson, 2010). Therefore, to understand the area distribution of the glaciers with elevation, we computed glacier mass balance of all investigated glaciers in this region and their dependency with glacier area and median elevation (Fig. 10, Fig. 11A & 11B). We observed (Fig. 10) that the glaciers in the study region lost ~0.75 m a^{-1} (46% more than average downwasting of ~0.51 m a^{-1}) ice during 2000–2020 within the median elevation of 4400–5600 m. Moreover, only ~14% glacier area contributed an average downwasting of ~0.80 m a^{-1}, ~57% higher than the average downwasting rate, in the lowest 500 m elevation range (4400–4900 m). A similar trend of average ice loss was also evident for debris cover (~0.74 m a^{-1}) and clean ice glaciers (~0.52 m a^{-1}) during the same time period (2000–2020) in lower median elevation range (4400–5600 m). However, the downwasting rate was more severe over debris covered glaciers (45% more than average downwasting) as compared to clean ice glacier (22% more than average downwasting). Further, we analyzed the correlation between glacier mass balance of all investigated glaciers and glacier median elevation (Fig. 11A, Supplementary Fig. 2A & 3A). The regional glacier mass budget showed significant correlation ($r = 0.15$ and $p = 0.03$) with median elevation and we also observed similar correlation by both clean ice ($r = 0.11$ and $p = 0.04$) and debris cover glaciers ($r = 0.21$ and $p = 0.01$). The positive correlation between mass balance with median glacier altitude emphasizes that high-altitude glaciers are less affected by regional mass loss probably due to the increased precipitation with relatively low temperature at higher altitudes, also reported by Zhao et al. (2016) in other part of HMA, which favors enhanced accumulation compared to low-altitude glaciers.

Similar to the studies conducted on Swiss-Alps (Paul and Haeberli, 2008; Huss, 2012), we also did not find any significant statistical correlation (Fig. 11B, Supplementary Fig. 2B & 3B) between the glacier mass budget with glacier area ($r = 0.09$ and $p = 0.20$), however, it was evident that larger glaciers (>5 km^2) have lost slightly more ice, with an average of ~0.54 m a^{-1}, as compared to smaller glaciers (~0.42 m a^{-1} < 0.25 km^2). The average ice thickness of the smaller glaciers in this region during 2000 (Farinotti et al., 2019) was estimated as 16.3 ± 5.8 m which was much less than the average ice thickness of bigger glaciers (97.9 ± 28.8 m). Our mass balance estimates indicate an average thickness loss of 18.7 ± 2.52 m between 1973 and 2020. Therefore, it can be anticipated that by the time the next geodetic measurements are

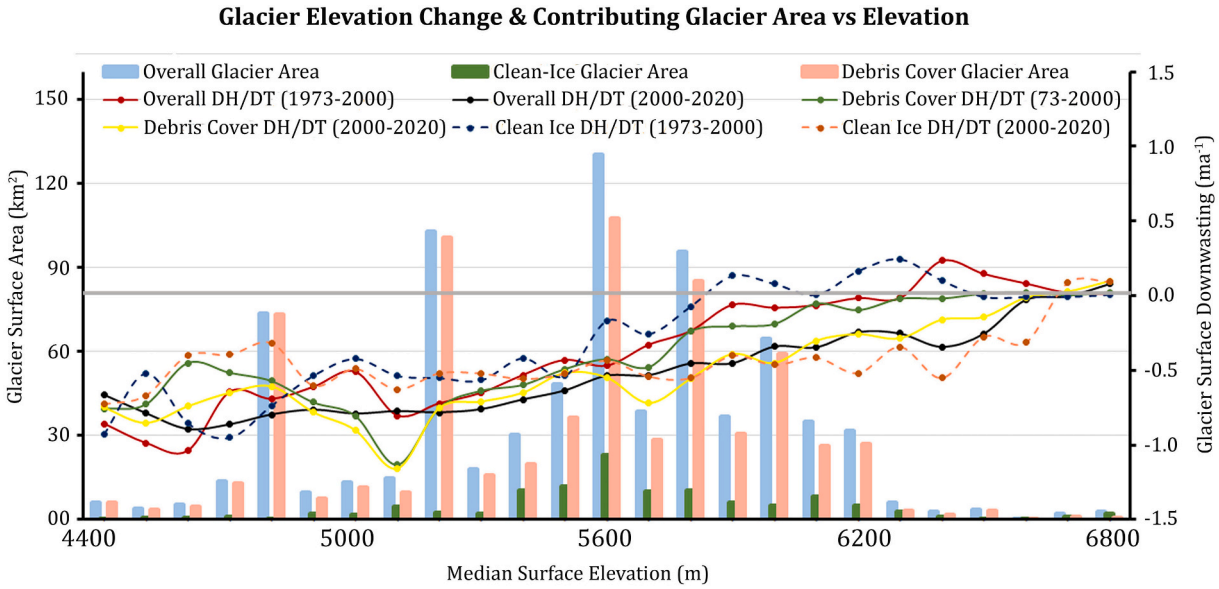

Fig. 10. Temporal variation of glacier surface downwasting and corresponding glacier area contribution with median elevation distribution of the entire study area.

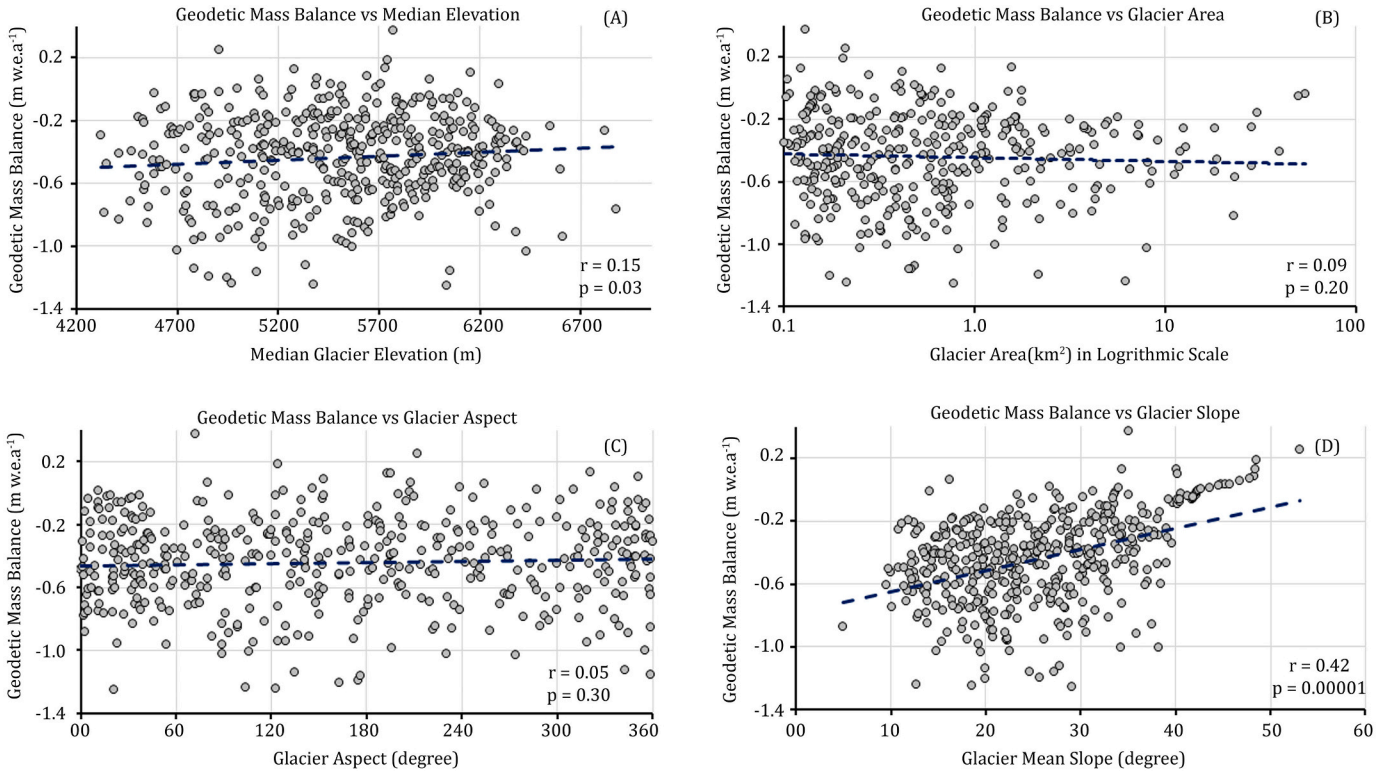

Fig. 11. Geodetic mass balance for all the investigated glaciers as a foundation of four morphological parameters (A) median elevation (B) glacier surface area (C) glacier aspect and (D) glacier slope. Correlation-coefficient (r) and their significance (*p*-value) are also provided for each of the variables.

made, many of the small glaciers' beds might have already been exposed, so that no ice remained to be melted, resulting in less thickness change and further mass loss (Hoelzle et al., 2003; Paul and Haeberli, 2008).

6.3.1.2. Glacier aspect. The orientation of the glacier surface determines the amount of solar radiation it receives. In general, mean daily temperatures and accumulated temperatures in spring and early summer are higher on south facing slopes, leading to a more enhanced melting and ablation, whereas north facing slopes receive less sunlight and preserve more snow and ice (Cuffey and Paterson, 2010). We didn't observe any significant statistical correlation (Fig. 11C, Supplementary Fig. 2C & 3C) between glacier mass balance with their aspect ($r = 0.05$ and $p = 0.3$). This could be the result of taking the glaciers' mean aspect into account rather than their terminal aspect, where ablation primarily takes place. However, we found that the northern aspect glaciers lost slightly more (-0.42 m w.e. a^{-1}) as compared to the south oriented glaciers (-0.36 m w.e. a^{-1}) during 2000–2020. Thus, it can be stated that mean aspect does not play a major role in controlling glacier mass budget.

6.3.1.3. Glacier slope. The slope of a glacier also affects its mass balance by influencing the amount of solar radiation received on different parts of the glacier. Radiation intensity varies with slope and differences due to aspect are more pronounced on steeper slopes. However, in valleys, due to the effect of shading, the relationships are often more complex and may control the melt patterns in a different way (Hock, 1999; Saydi and Ding, 2020). Slope also affects the flow dynamics of the glaciers with steeper slopes increasing the glacier flow. This, in turn, impact the redistribution of ice and affect mass balance.

We observed (Fig. 11D & Supplementary Fig. 2D & 3D) that the mean slope for all glaciers ($r = 0.42$ and $p = 0.00001$), clean ice (r = 0.42 and p = 0.00001) and debris cover ($r = 0.30$ and $p = 0.0002$) glaciers had significant correlation with the average glacier mass balance, however, considering the terminus slope of each glacier, we didn't observe any significant difference of their correlation ($r = 0.48$ and p = 0) in our study region.

The positive correlation between mass balance with mean glacier slope emphasized that steep glaciers are less affected by regional mass loss (Fischer et al., 2015; Rabatel et al., 2016; Brun et al., 2019; Davaze et al., 2020). This is primarily due to glaciers with higher slopes and in effect, higher flow dynamics, results in a higher ice flux (Davaze et al., 2020). Therefore, steep glaciers have the ability to regain their balance state more quickly and resist further mass loss. On the contrary, low slope glaciers remain in imbalance for much longer time probably because they are unable to adjust their geometry to reach a new equilibrium as fast as the steeper glaciers and undergo significant mass loss. Moreover, glacier with low slopes and long tongues at lower elevations in HMA are in a tendency of having more debris cover, and we observed in this study that debris-covered glaciers are losing significantly more ice in this region as also reported elsewhere (Gardelle et al., 2013; King et al., 2019).

6.3.2. Glacier ice dynamics and glacier surging

Ice dynamics refers to the flow of ice within a glacier and can control the mass balance significantly. We plotted the average flow velocities of different glaciers across mass budget (Supplementary Fig. 4A). We examine glaciers with an area of >1 km^2 with the maximum glacier area being 53.9 km^2. We observe that there is a tendency of increasing positive mass budget with the increase in mean velocity of the glaciers (Supplementary Fig. 4). However, the relationship is not statistically significant ($r = 0.03$ and $p = 0.77$) as many of the smaller glaciers do not follow this response pattern.

Glacier ice dynamics also influence individual glaciers mass balance. Glacier surface velocities provide insight into glacier dynamics and can be used to identify surging glaciers in their active phase of surging. We identified surge-type behaviour of a glacier (Glacier −1 in Fig. 1; RGI60–14.26971) in our study area. This glacier was identified as a

surge-type glacier by Guillet et al. (2022) and Bhambri et al. (2023) but no detailed investigations were performed. Surge activity usually depends on dynamic instabilities due to internal and sub-glacial conditions (Dolgoushin and Osipova, 1975; Sharp et al., 1988) and are unrelated to or only indirectly dependent on external triggers (Meier and Post, 1969; Quincey and Luckman, 2014). A glacier surge is normally initiated due to the increased ice accumulation in the reservoir region of a glacier resulting in an increased pressure on the glacier bed. As a result, the water in the glacier bed may increase which promotes the surge activity by reducing friction with the bed (Kamb, 1987; Björnsson, 1998; Barrand and Murray, 2006). The increased pressure may also deform the sediments in the glacier bed, thereby enhancing surge activity (Murray et al., 2000). In both cases, the glacier experiences an increase in overall velocity. Here, we have also observed around seven times increase in glacier velocity during the surge activity (Fig. 12) and corresponding heterogeneous mass budget before (-0.19 ± 0.07 m w.e. a^{-1} during 2000–2018) and after (-0.40 ± 0.06 m w.e. a^{-1} during 2018–2021) the surge. The typical pattern of surge could be confirmed also analyzing ICESat-2 (Supplementary Fig. 5A). A distinct drop in surface elevation in the source area and rise in the area close to terminus between 2019 and 2021 is also evident (Supplementary Fig. 5B). This corresponds to the results from both the DEM differecing and analysis of surface velocity (Fig. 12). Similar low mass loss rates in the late quiescence period and then substantially greater mass loss rates during the surge were also evident in other parts of the Tibetan plateau (King et al., 2023).

Apart from heterogeneous mass budget, the glacier also experienced variable length fluctuation during the study period (Fig. 12). The glacier retreated by 310 ± 8.2 m from 1973 until 2019 and the glacier terminus was almost stagnant from 2018 to September 2019. Ice mass redistribution from the glacier's higher reaches has begun by this point and crevasses started forming near the terminus (Supplementary Fig. 6). This increased mass near the tongue then suddenly experienced a very rapid advancement of 796 ± 29.7 m within three months (until 3rd Dec 2019). The width of the glacier also increased considerably due to the transfer of ice from the upper reaches of the glacier (Supplementary Fig. 6). Overall, the glacier advanced by nearly 900 m from 2019 until the end of the study period, though the rate of advance is much decreased after 2019 (29.3 ± 4.10 m a^{-1}). Based on its rapid advancement (>100 m a^{-1}), we classify it as a confirmed surge-type glacier with surge index of 1, following the classification scheme of Mukherjee et al., 2017.

We also compared the ice thicknesses (bedrock topography based on Farinotti et al., 2019) before (2018) and after the surge (2020) along the centreline profile of the glacier. The reduction of ice thickness in the upper reaches of the glacier began in 2018, with an average minimum thickness of ~120 m (Fig. 12E). The ice thickness reductions in the reservoir area continued through 2020, and the 2020 DEM indicates minimum average thickness in the reservoir area was ~74 m, implying considerable ice mass redistribution from this area down glacier, resulting in an advance of the glacier. By 2021, the glacier has started accumulating ice again in its reservoir area (average thickness ~ 91 m), which is evident from the increase in thickness in this area (Fig. 12E), while still advancing at a much-reduced rate (Fig. 12A). The retreat from 1973 to 2019 implies that the glacier has a surge cycle of >45 years, and we may not observe a surge event for this glacier in the next few decades. Such long quiescent phases were observed for many surge-type glaciers in the Tien Shan region (Mukherjee et al., 2017).

We also estimated geometries such as length, area, elevation range and slope of this surge type glacier and compared with the normal glacier and found mean percentile scores of 96.4, 97.5, 92.8 and 15.9 respectively. These results also emphasized the fact that surge-type glaciers are generally larger than most non-surging glaciers and have shallower slopes (Sevestre and Benn, 2015; Mukherjee et al., 2017). Therefore, the evidence from the geometries together with the similar temperature and precipitation trend, (annual precipitation and

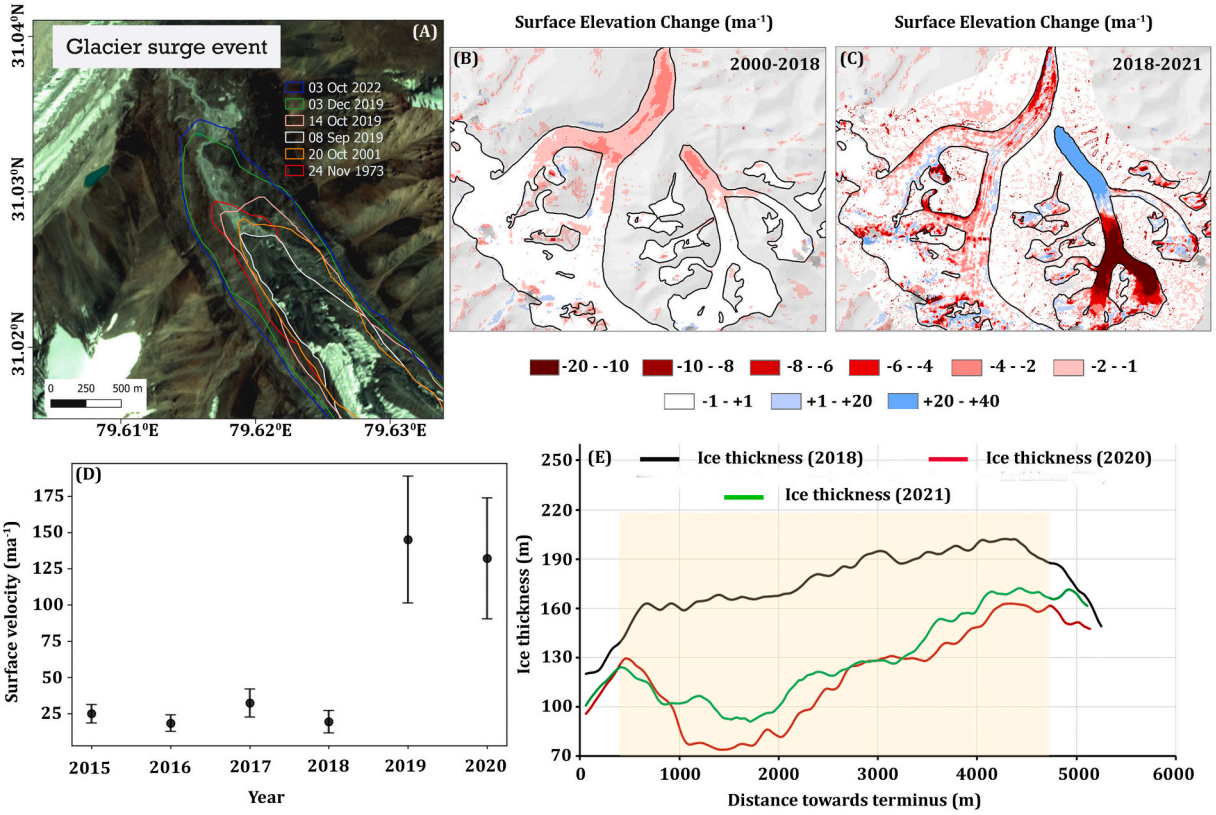

Fig. 12. (A) Glacier extent in pre-surge and during the surge for different time periods of glacier RGI60–14.26971 (background image: PlanetScope scene of 8th September 2019). Elevation change (B) before the surge activity, (C) after the surge activity, (D) Annual mean surface velocity derived from Sentinel-1 data of the surge type glacier and (E) Thickness profile along the center flow line towards the terminus of the surge type glacier in different time period.

temperature ~ 1260 mm a^{-1} and ~ −5.5 °C) where most of the surge type glaciers are found (Sevestre et al., 2015), might enhance the chance of surging in this region also in near future.

6.3.3. Debris cover and dynamic separation

We observed that the debris cover portions of all the investigated glaciers lost more than ~56% (−0.81 ± 0.13 m a^{-1}) ice compared to the overall average ice loss (−0.52 ± 0.10 m a^{-1}) during 2000–2020. It was also observed that the increased debris thickness reduced glacier mass loss ($r = 0.16$ and $p = 0.03$) (Supplementary Fig. 4B). Typically, thin debris enhances melting rate by reducing the glacier albedo and absorbing more incoming solar radiation (Østrem, 1959), whereas, thick debris increases the surface temperature, thereby increasing both the outgoing longwave radiation and turbulent energy fluxes and reduce the melting (Steiner et al., 2018). However, apart from the debris thickness, several other factors, such as, presence of supra glacial lake, ponds, ice-cliffs, distribution of the debris, size and composition of the debris particles, and the local climatic conditions also influence the glacier mass balance (Benn et al., 2012; Ragettli et al., 2016; Kneib et al., 2021; Bhambri et al., 2023), which needs to be investigated further.

Debris cover on glaciers also lead to differential melting rates and flow patterns which creates variations in surface topography, with depressions forming in the areas of faster melting and debris cover mounds or hummocks developing in the areas of slower melting. These irregularities may hamper the smooth flow of ice, creating complex pattern of ice movement, which may lead to dynamic separation of the glacier (e.g. Benn et al., 2012). In addition, debris cover may also increase the shear stress that increases the strain rates. Such differential strain rates may cause the glacier to separate into distinct sections with different flow characteristics (Jennings and Hambrey, 2021).

We observe one such likely dynamic separation phenomenon for Raj Bank Glacier (RGI60–15.06559) in our study area. A prominent bedrock ridge is now growing, which might separate the debris-covered tongue of Raj Bank Glacier (RGI60–15.06559) from two clean ice accumulation zones in near future, where two tributary flow units converge in the central portion of the glacier, with mean elevation of ~5600 and ~5200 m a.s.l. respectively. The surface elevation rapidly drops from 5600 m to 4845 m over a short distance of ~100 m from upper accumulation region. A previous study reported (Pandey et al., 2022) that the glacier is continuously decreasing in area (2.43 ± 1.31%) and snowline altitude (SLA) has also shifted upwards by 330 ± 63 m during 1962 to 2019. Interestingly, in this zone a bedrock wall began to emerge in ~1990, which was not evident in 1973. The exposure of this bed rock wall started spreading along the width of the glacier which may have impacted its flow regime and the movement of ice mass to its lower reaches (Supplement Fig. 4). Additionally, a large ice-cliff, which formed between 2000 and 2006 (Supplement Fig. 4), has now expanded to almost cover the full width of the glacier, which may have been responsible for the stagnant nature of the ice immediately down-glacier of the bedrock outcrop and is likely to have promoted downwasting in ablation region. Therefore, the lower reaches of this glacier are likely to suffer greater ice mass loss in near future due to the deficit of ice transport from the upstream region. Further investigation and constant monitoring is required to understand the long-term behaviour of this glacier. A comprehensive detail of the phenomenon based on time-series analysis of the satellite images is provided in supplement (Supplementary note 3).

6.4. Implication of glacier behaviour in the wider Himalayan region

Our temporally detailed measurements of glacier change offer a comprehensive view of glacier evolution in the Alaknanda Basin, but can also be used to inform on the likely behaviour of glaciers elsewhere in the Himalaya and whole HMA which have experienced similar changes in climate recently. Regional remotely sensed observations suggest that contemporary (post-2000) glacier mass budgets are relatively consistent along the Himalaya, with several studies estimating that glaciers at the source of rivers such as the Indus and the Ganges lost ice mass at a rate of −0.30 to −0.40 m w.e. a^{-1} from 2000 to 2020 (Brun et al., 2017; Shean et al., 2020). Our multi-temporal mass budget results offer a clear indication that recent glacier mass budgets are substantially more negative (−0.68 ± 0.09 m w.e. a^{-1}) than indicated by studies which have averaged results over longer time periods. If this is the general trend in the wider HMA region then we would expect glaciers in the broader region to have experienced similar multi-temporal mass balance perturbations within the last decades. In the period 1973 to 2020, these glaciers lost 12.9 ± 1.7 Gt, which accounts for up to 0.036 ± 0.006 mm sea level rise, considering an ocean surface area of 3.6×10^{14} m^2 (Amante, 2009). Studies such as Dimri et al. (2018) indicate significant contemporary warming, which may continue until at least the end of 21st century (Dimri et al., 2018) if the current trend of temperature increase continues that we have observed in the recent decades (Fig. 8). By combining multi-temporal mass budget results with multi-temporal climate parameters like summer temperature, winter precipitation, annual temperature and annual snowfall, we observed that summer temperature has most control on the region wide glacier mass balance. We obtained a regional mass balance sensitivity of −0.6 m w.e. a^{-1} °C^{-1}, and came up with a relationship of glacier mass balance and average summer temperature of the study region. This relationship can be used to generate a long-term mass balance time series of the glaciers of this region. Based on these values, we can comment on the yearly glacier meltwater runoff component during the last decades. Similar studies in other parts of the world and on individual glaciers may help to establish relationships with climate variables, reconstruct glacier mass balance series, and will improve our understanding on the response of glaciers in different parts of the world to a changing climate.

The prolonged thinning of Raj Bank Glacier may lead to its separation into two dynamically contrasting bodies of ice with an effectively stagnant glacier tongue now downwasting at an accelerated pace, below a still actively flowing accumulation zone. The dynamic separation of long, gently sloping debris-covered glaciers is a scenario that has been predicted elsewhere in HMA (Rowan et al., 2015, 2021) and our observations of this style of glacier evolution indicate that this style of glacier recession could be widespread in the future. This has implications not only for modelling studies that aim to simulate glacier mass loss and subsequent meltwater yield, but also complicates the prediction of glacial lake development and associated hazard (Glacial Lake Outburst Flood) potential. Stagnant, gently sloping, debris-covered glacier tongues are hotspots of supraglacial pond formation and lake development (Quincey et al., 2007; King et al., 2018) and these conditions may soon be prevalent on glaciers such as Raj Bank Glacier.

Finally, the in such detail previously undocumented surge-type behaviour of glacier RGI60–14.26971 emphasizes the findings of Guillet et al. (2022) that surge-type glaciers are much more common than previously thought in HMA. Our results, in combination with the inventory of Guillet et al. (2022), show how the surge of RGI60–14.26971 is not an isolated example of glacier surging in the Western Himalaya. Indeed, the climate in this region fits the envelope described by Sevestre and Benn (2015) within which surge-type glaciers typically occur and it should therefore be expected that further glacier surging may occur in the region. We used purely remotely-sensed observation to identify and study this surge, which shows how remote sensing has become a valuable technique for monitoring surge behaviour when logistically difficult field-based observations are not practical. Despite the fact that the repeat observations of global glacier surface elevation change data (Hugonnet et al., 2021) might offer a great synoptic overview of the glacier states, but this elevation change grid would not always be able to capture the rapid advance/retreat and related mass changes during for example, surge events, if the glacier extents are kept unchanged over the period of observation. Therefore, muti-temporal regional area change and mass balance data in combination with global mass balance (Hugonnet et al., 2021) and glacier flow (Gardner et al., 2019; Friedl

et al., 2021) data will aid the identification of surge-related glacier hazards across HMA, which will help monitoring, forecast and mitigation of related hazards (e.g. Gao et al., 2021).

7. Conclusions

We studied the long-term behaviour of 445 glaciers in the Alaknanda basin and its surroundings over the period of 1973–2020. Before 2000 (1973–2000), the mean glacier mass balance in the region was -0.30 ± 0.12 m w.e. a^{-1}. This decreased to -0.43 ± 0.06 m w.e. a^{-1} during 2000–2020. There was heterogeneous mass loss both in spatial and temporal scales and mass loss has increased significantly in our most recent study period (-0.68 ± 0.09 m w.e. a^{-1} in 2015–2020). Our multi-temporal geodetic observations are capable of quantifying changes in glacier surface elevation which are masked in longer term, but less temporally resolved datasets. Time series of temperature, precipitation and snowfall available from ERA5 Land data indicates a significant increase in summer and autumn temperature during recent time periods in the region. The prolonged ablation season due to significant seasonal temperature increases has likely enhanced glacier mass loss in the recent periods. ERA5 Land precipitation data did not show any significant trend throughout the observation period but solid precipitation in the spring season reduced by ~28.6% during 2015–2020 perhaps contributing to a reduction in the winter accumulation. Apart from climatic factors, non-climatic factors also influenced regional glacier mass loss. Steep and higher elevation glaciers in this region were less affected by the changing climate, perhaps due to more accumulation and rapid transfer of snow and ice that helped them to readjust their geometry with the ongoing climate change compared to low slope/less dynamic glaciers. We identified a surge-type glacier in the study region that advanced rapidly (800 m) within three months between Sep-Dec 2019. The advance is still ongoing 2023, though at a much-reduced rate. Analysis of available images suggests that the quiescent phase for this glacier is >45 years. Our study highlighted that factors such as morphometry and topographic features can also potentially influence negative impact of regional glacier mass balance which may become amplified in coming decades. These multi-temporal mass budget estimates also provide us with an option to generate annual mass balance time series and quantify possible regional mass budgets for future climate scenarios. Finally, though the non-climatic factors also influenced glacier mass budget in this study, but the results indicate that average summer temperature has the strongest influence on mass budget.

Authors contributions

A.B, K.M, O.K & T.B design the study; A.B generated all Digital Elevation Models (DEM); A.B analyzed all the mass balance data and prepared the supplement figures and tables; A.B generated glacier outlines; K.M & A.B processed and analyzed all the ERA5 Land climate data and produced the graphs for all climate data; K.M analyzed surging glacier and generate figures related to surging; S·K analyzed all Meteorological station data; JK analysed the ICESat-2 data for the surge-type glacier; A.B, O.K, K.M, S.N.R, A.V.K, J.K & T.B analysed the final results; A.B led the writing of the paper and all other co-authors contributed to refining the manuscript.

Funding statement

A.B acknowledge the research funding (grant no. CRG/2021/002450) received from Department of Science & Technology (DST), India, under Core Research Grant (CRG). K.M acknowledges support from Constructing a Digital Environment (CDE) project funded by Natural Environment Research Council (NERC grant no. NE/S016287/1).

Declaration of Competing Interest

The authors declare that they have no known competing financial interests or personal relationships that could have appeared to influence the work reported in this paper.

Data availability statement

All data which is not restricted by license agreements (e.g. the original satellite) will be made available in the public domain. Additionally, all the data will be also available to the international community through the MountCryo (www.mountcryo.org/dataset/) data portal. The ERA5 Land reanalysis data can be found at https://climate.copernicus.eu/climate-reanalysis.

Acknowledgements

We greatly acknowledge the constructive comments from the anonymous reviewers that helped improve the quality of the manuscript significantly. We are grateful to the satellite data providers: USGS for Landsat, and JPL/NASA and METI for ASTER. We are grateful to CNES/Airbus DS for the provision of the Pléiades satellite data within the ISIS program (Pleiades (c) CNES (2018), Distribution Airbus DS). The ERA 5 reanalysis was made available by courtesy of ECMWF/Copernicus.

Appendix A. Supplementary data

Supplementary data to this article can be found online at https://doi.org/10.1016/j.gloplacha.2023.104260.

References

Abermann, J., Kuhn, M., Fischer, A., 2011. Climatic controls of glacier distribution and glacier changes in Austria. Ann. Glaciol. 52 (59), 83–90. https://doi.org/10.3189/172756411799096222.

Amante, C., 2009. ETOPO1 1 Arc-Minute Global Relief Model: Procedures, Data Sources and Analysis. National Ocean and Atmospheric Administration, Washington, DC.

Azam, M.F., Ramanathan, A.L., Wagnon, P., Vincent, C., Linda, A., Berthier, E., Sharma, P., Mandal, A., Angchuk, T., Singh, V.B., Pottakkal, J.G., 2016. Meteorological conditions, seasonal and annual mass balances of Chhota Shigri Glacier, Western Himalaya, India. Ann. Glaciol. 57 (71), 328–338. https://doi.org/10.3189/2016AoG71A570.

Azam, M.F., Wagnon, P., Berthier, E., Vincent, C., Fujita, K., Kargel, J.S., 2018. Review of the status and mass changes of Himalayan-Karakoram glaciers. J. Glaciol. 64 (243), 61–74. https://doi.org/10.1017/jog.2017.86.

Bandyopadhyay, D., Singh, G., Kulkarni, A.V., 2019. Spatial distribution of Decadal Ice-thickness change and glacier stored water loss in the upper Ganga Basin, India during 2000–2014. Sci. Rep. 9 (1), 16730. https://doi.org/10.1038/s41598-019-53055-y.

Banerjee, A., Shankar, R., 2013. On the response of Himalayan glaciers to climate change. J. Glaciol. 59 (215), 480–490. https://doi.org/10.3189/2013JoG12J130.

Barrand, N.E., Murray, T., 2006. Multivariate controls on the incidence of glacier surging in the Karakoram Himalaya. Arct. Antarct. Alp. Res. 38 (4), 489–498. https://doi.org/10.1657/1523-0430(2006)38[489:MCOTIO]2.0.CO;2.

Basistha, A., Arya, D.S., Goel, N.K., 2009. Analysis of historical changes in rainfall in the Indian Himalayas. Int. J. Climatol. 29 (4), 555–572. https://doi.org/10.1002/joc.1706.

Benn, D.I., Bolch, T., Hands, K., Gulley, J., Luckman, A., Nicholson, L.I., Quincey, D., Thompson, S., Toumi, R., Wiseman, 2012. Response of debris-covered glaciers in the Mount Everest region to recent warming, and implications for outburst flood hazards. Earth Sci. Rev. 114 (1–2), 156–174. https://doi.org/10.1016/j.earscirev.2012.03.008.

Berthier, E., Arnaud, Y., Kumar, R., Ahmad, S., Wagnon, P., Chevallier, P., 2007. Remote sensing estimates of glacier mass balances in the Himachal Pradesh (Western Himalaya, India). Remote Sens. Environ. 108, 327–338. https://doi.org/10.1016/j.rse.2006.11.017.

Bhambri, R., Bolch, T., Chaujar, R.K., Kulshreshtha, R.C., 2011. Glacier changes in the Garhwal Himalaya, India, from 1968 to 2006 based on remote sensing. J. Glaciol. 57 (203), 543–556. https://doi.org/10.3189/002214311796905604.

Bhattacharya, A., Bolch, T., Mukherjee, K., Pieczonka, T., Kropáček, J., Buchroithner, M. F., 2016. Overall recession and mass budget of Gangotri Glacier, Garhwal Himalayas, from 1965 to 2015 using remote sensing data. J. Glaciol. 62 (236), 1115–1133. https://doi.org/10.1017/jog.2016.96.

Bhambri, R., Schmidt, S., Chand, P., Nüsser, M., Haritashya, U., Sain, K., Tiwari, S.K., Yadav, J.S., 2023. Heterogeneity in glacier thinning and slowdown of ice movement

in the Garhwal Himalaya, India. Sci. Total. Environ. 875, 162625. https://doi.org/10.1016/j.scitotenv.2023.162625.
Bhattacharya, A., Bolch, T., Mukherjee, K., King, O., Menounos, B., Kapitsa, V., Neckel, N., Yang, W., Yao, T., 2021. High mountain asian glacier response to climate revealed by multi-temporal satellite observations since the 1960s. Nat. Commun. 12 (1), 4133. https://doi.org/10.1038/s41467-021-24180-y.
Bhushan, S., Syed, T.H., Arendt, A.A., Kulkarni, A.V., Sinha, D., 2018. Assessing controls on mass budget and surface velocity variations of glaciers in Western Himalaya. Sci. Rep. 8 (1), 8885. https://doi.org/10.1038/s41598-018-27014-y.
Bhutiyani, M.R., Kale, V.S., Pawar, N.J., 2010. Climate change and the precipitation variations in the Northwestern Himalaya: 1866–2006. Int. J. Climatol. 30 (4), 535–548. https://doi.org/10.1002/joc.1920.
Biemans, H., Siderius, C., Lutz, A.F., Nepal, S., Ahmad, B., Hassan, T., von Bloh, W., Wijngaard, R.R., Wester, P., Shrestha, A.B., Immerzeel, W.W., 2019. Importance of snow and glacier meltwater for agriculture on the Indo-Gangetic Plain. Nat. Sustain. 2 (7), 594–601. https://doi.org/10.1038/s41893-019-0305-3.
Björnsson, H., 1998. Hydrological characteristics of the drainage system beneath a surging glacier. Nature 395 (6704), 771–774. https://doi.org/10.1038/27384.
Bolch, T., Buchroithner, M.F., Kunert, A., Kamp, U., 2007. Automated delineation of debris-covered glaciers based on ASTER data. In: Gomarasca, M.A. (Ed.), GeoInformation in Europe. Proceedings of the 27th EARSeL Symposium, 4–7 June, 2007, Bozen, Italy. Millpress, Rotterdam, pp. 403–410.
Bolch, T., Pieczonka, T., Benn, D.I., 2011. Multi-decadal Mass loss of glaciers in the everest area (Nepal Himalaya) derived from stereo imagery. Cryosphere. 5 (2), 349–358. https://doi.org/10.5194/tc-5-349-2011.
Bolch, T., Kulkarni, A.V., Kääb, A., Huggel, C., Paul, F., Cogley, J.G., Frey, H., Kargel, J. S., Fujita, K., Scheel, M., Bajracharya, S., Stoffel, M., 2012. The state and fate of Himalayan Glaciers. Science 336 (6079), 310–314. https://doi.org/10.1126/science.1215828.
Bolch, T., Shea, J.M., Liu, S., Azam, F.M., Gao, Y., Gruber, S., Immerzeel, W.W., Kulkarni, A.V., Li, H., Tahir, A.A., Zhang, G., Zhang, Y., 2019. Status and change of the cryosphere in the extended Hindu Kush Himalaya region. In: Wester, P., Mishra, A., Mukherji, A., Shrestha, A. (Eds.), The Hindu Kush Himalaya Assessment. Springer, Cham, pp. 209–255. https://doi.org/10.1007/978-3-319-92288-1_7.
Braithwaite, R., 2009. After six decades of monitoring glacier mass balance, we still need data but it should be richer data. Ann. Glaciol. 50 (50), 191–197. https://doi.org/10.3189/172756409787769573.
Braithwaite, R., Raper, S., 2009. Estimating equilibrium-line altitude (ELA) from glacier inventory data. Ann. Glaciol. 50 (53), 127–132. https://doi.org/10.3189/172756410790595930.
Brown, D.C., 1971. Close-range camera calibration. Photogramm. Eng. Remote. Sens. 37 (8), 855–866.
Brun, F., Berthier, E., Wagnon, P., Kääb, A., Treichler, D., 2017. A spatially resolved estimate of high mountain asia glacier mass balances from 2000 to 2016. Nat. Geosci. 10 (9), 668–673. https://doi.org/10.1038/ngeo2999.
Brun, F., Wagnon, P., Berthier, E., Jomelli, V., Maharjan, S.B., Shrestha, F., Kraaijenbrink, P.D.A., 2019. Heterogeneous influence of glacier morphology on the mass balance variability in high mountain Asia. Case Rep. Med. 124 (6), 1331–1345. https://doi.org/10.1029/2018JF004838.
Chaturvedi, R.K., Joshi, J., Jayaraman, M., Bala, G., Ravindranath, N.H., 2012. Multi-model climate change projections for India under representative concentration pathways. Curr. Sci. 103 (7), 791–802.
Clarke, G.K.C., Jarosch, A.H., Anslow, F.S., Radic, V., Menounos, B., 2015. Projected deglaciation of western Canada in the twenty-first century. Nat. Geosci. 8, 372–377. https://doi.org/10.1038/ngeo2407.
Cuffey, K., Paterson, W., 2010. The Physics of Glaciers. Elsevier, Burlington, MA, USA, ISBN 978-0-12-369461-4.
Davaze, L., Rabatel, A., Dufour, A., Hugonnet, R., Arnaud, Y., 2020. Region-wide annual glacier surface mass balance for the European Alps from 2000 to 2016. Front. Earth Sci. 8, 149. https://doi.org/10.3389/feart.2020.00149.
Dehecq, A., Gourmelen, N., Gardner, A.S., Brun, F., Goldberg, D., Nienow, P.W., Berthier, E., Vincent, C., Wagnon, P., Trouve, E., 2019. Twenty-first century glacier slowdown driven by mass loss in high mountain Asia. Nat. Geosci. 12 (1), 22–27. https://doi.org/10.1038/s41561-018-0271-9.
Dimri, A.P., Kumar, D., Choudhary, A., Maharana, P., 2018. Future changes over the Himalayas: mean temperature. Glob. Planet. Chang. 162, 235–251. https://doi.org/10.1016/j.gloplacha.2018.01.014.
Dobhal, D.P., Gergan, J.T., Thayyen, R.J., 2008. Mass balance studies of the Dokriani Glacier from 1992 to 2000. Bull. Glaciol. Res. 25, 9–17.
Dobhal, D.P., Mehta, M., Srivastava, D., 2013. Influence of debris cover on terminus retreat and mass changes of Chorabari Glacier, Garhwal Region, Central Himalaya, India. J. Glaciol. 59 (217), 961–971. https://doi.org/10.3189/2013JoG12J180.
Dolgoushin, L.D., Osipova, G.B., 1975. Glacier surges and the problem of their forecasting. IAHS Publ. 104, 292–304.
Farinotti, D., Huss, M., Fürst, J.J., Landmann, J., Machguth, H., Maussion, F., Pandit, A., 2019. A consensus estimate for the ice thickness distribution of all glaciers on earth. Nat. Geosci. 12 (3), 168–173. https://doi.org/10.1038/s41561-019-0300-3.
Fischer, M., Huss, M., Hoelzle, M., 2015. Surface elevation and mass changes of all Swiss Glaciers 1980–2010. Cryosphere. 9 (2), 525–540. https://doi.org/10.5194/tc-9-525-2015.
Friedl, P., Seehaus, T., Braun, M., 2021. Global time series and temporal mosaics of glacier surface velocities derived from Sentinel-1 Data. Earth Syst. Sci. Data 13 (10), 4653–4675. https://doi.org/10.5194/essd-13-4653-2021.
Gao, Y., Liu, S., Qi, M., Xie, F., Wu, K., Zhu, Y., 2021. Glacier-related hazards along the International Karakoram highway: status and future perspectives. Front. Earth Sci. 9, 611501. https://doi.org/10.3389/feart.2021.611501.
Gardelle, J., Berthier, E., Arnaud, Y., Kääb, A., 2013. Region-wide glacier mass balances over the Pamir-Karakoram-Himalaya during 1999–2011. Cryosphere. 7 (4), 1263–1286. https://doi.org/10.5194/tc-7-1263-2013.
Gardner, A.S., Fahnestock, M.A., Scambos, T., 2019. ITS_LIVE Regional Glacier and Ice Sheet Surface Velocities. Data archived at National Snow and Ice Data centre. https://doi.org/10.5067/6II6VW8LLW.
Gautam, C.K., Mukherjee, B.K., 1992. Synthesis of Glaciological Studies on Tipra Bank glacier, Bhyundar Gan ga Basin, District Chamoli, Uttar Pradesh (F.S. 1980–1988). Geological Survey of India, Lucknow.
Gornall, J., Betts, R., Burke, E., Clark, R., Camp, J., Willett, K., Wiltshire, A., 2010. Implications of climate change for agricultural productivity in the early twenty-first century. Philos. Trans. R. Soc. Lond. Ser. B Biol. Sci. 365 (1554), 2973–2989. https://doi.org/10.1098/rstb.2010.0158.
Grodechi, J., Dial, G., 2003. Block adjustment of high-resolution satellite images described by rational polynomials. Photogramm. Eng. Remote. Sens. 69, 59–68.
Guillet, G., King, O., Lv, M., Ghuffar, S., Benn, D., Quincey, D., Bolch, T., 2022. A regionally resolved inventory of High Mountain Asia surge-type glaciers, derived from a multi-factor remote sensing approach. Cryosphere 16, 603–623. https://doi.org/10.5194/tc-16-603-2022.
Hall, D.K., Bayr, K.J., Schöner, W., Bindschadler, R.A., Chien, J.Y.L., 2003. Consideration of the errors inherent in mapping historical glacier positions in Austria from the ground and space (1893–2001). Remote Sens. Environ. 86 (4), 566–577. https://doi.org/10.1016/S0034-4257(03)00134-2.
Hirschmuller, H., 2007. Stereo processing by semiglobal matching and mutual information. IEEE Trans. Pattern Anal. Mach. Intell. 30 (2), 328–341. https://doi.org/10.1109/TPAMI.2007.1166.
Hock, R., 1999. A distributed temperature-index ice- and snowmelt model including potential direct solar radiation. J. Glaciol. 45 (149), 101e111. https://doi.org/10.1017/s0022143000003087.
Hock, R., Bliss, A., Marzeion, B.E.N., Giesen, R.H., Hirabayashi, Y., Huss, M., Radić, V., Slangen, A.B., 2019. GlacierMIP–A model intercomparison of global-scale glacier mass-balance models and projections. J. Glaciol. 65 (251), 453–467. https://doi.org/10.1017/jog.2019.22.
Hoelzle, M., Haeberli, W., Dischl, M., Peschke, W., 2003. Secular glacier mass balances derived from cumulative glacier length changes. Glob. Planet. Chang. 36 (4), 295–306. https://doi.org/10.1016/S0921-8181(02)00223-0.
Hugonnet, R., McNabb, R., Berthier, E., Menounos, B., Nuth, C., Girod, L., Farinotti, D., Huss, M., Dussaillant, I., Brun, F., Kääb, A., 2021. Accelerated global glacier Mass loss in the early Twenty-first century. Nature. 592 (7856), 726–731. https://doi.org/10.1038/s41586-021-03436-z.
Huss, M., 2012. Extrapolating glacier mass balance to the mountain-range scale: the European Alps 1900–2100. Cryosphere. 6 (4), 713–727. https://doi.org/10.5194/tc-6-713-2012.
Huss, M., 2013. Density assumptions for converting geodetic glacier volume change to mass change. Cryosphere. 7 (3), 877–887. https://doi.org/10.5194/tc-7-877-2013.
Huss, M., Hock, R., 2018. Global-scale hydrological response to future glacier mass loss. Nat. Clim. Chang. 8 (2), 135–140. https://doi.org/10.1038/s41558-017-0049-x.
Immerzeel, W.W., Lutz, A.F., Andrade, M., Bahl, A., Biemans, H., Bolch, T., Hyde, S., Brumby, S., Davies, B.J., Elmore, A.C., Emmer, A., Feng, M., Fernandez, A., Haritashys, U., Kargel, J.S., Koppes, M., Kraaijenbrink, P.D.A., Kulkarni, A.V., Mayewski, P.A., Nepal, S., Pacheco, P., Painter, T.H., Pellicciotti, F., Rajaram, H., Rupper, S., Sinisalo, A., Shrestha, A.B., Viviroli, D., Wada, Y., Xiao, C., Yao, T., Baillie, J.E.M., 2020. Importance and vulnerability of the world's water towers. Nature. 577 (7790), 364–369. https://doi.org/10.1038/s41586-019-1822-y.
Jennings, S.J.A., Hambrey, M.J., 2021. Structures and deformation in glaciers and ice sheets. Rev. Geophys. 59 https://doi.org/10.1029/2021RG000743 e2021RG000743.
Kamb, B., 1987. Glacier surge mechanism based on linked cavity configuration of the Basal Water Conduit System. J. Geophys. Res. Solid Earth 92 (B9), 9083–9100. https://doi.org/10.1029/JB092iB09p09083.
King, O., Dehecq, A., Quincey, D., Carrivick, J., 2018. Contrasting geometric and dynamic evaluation of lake and land-terminating glaciers in the central Himalaya. Glob. Planet. Chang. 167, 46–60. https://doi.org/10.1016/j.gloplacha.2018.05.006.
King, O., Bhattacharya, A., Bhambri, R., Bolch, T., 2019. Glacial lakes exacerbate Himalayan glacier mass loss. Sci. Rep. 9 (1), 1–9. https://doi.org/10.1038/s41598-019-53733-x.
King, O., Bhattacharya, A., Ghuffar, S., Tait, A., Guilford, S., Elmore, A.C., Bolch, T., 2020. Six decades of glacier mass changes around Mt. Everest are revealed by historical and contemporary images. One Earth 3 (5), 608–620. https://doi.org/10.1016/j.oneear.2020.10.019.
King, O., Ghuffar, S., Bhattacharya, A., Yao, R., Tandong, Y., Bolch, T., 2023. Glaciological and climatological drivers of heterogeneous glacier mass loss in the Tanggula Shan (Central-Eastern Tibetan Plateau), since the 1960s. J. Glaciol. 1-18 https://doi.org/10.1017/jog.2023.5.
Kneib, M., Miles, E.S., Jola, S., Buri, P., Herreid, S., Bhattacharya, A., Watson, C.S., Bolch, T., Quincey, D., Pellicciotti, F., 2021. Mapping ice cliffs on debris-covered glaciers using multispectral satellite images. Remote Sens. Environ. 253, 112201. https://doi.org/10.1016/j.rse.2020.112201.
Kraaijenbrink, P.D.A., Bierkens, M.F.P., Lutz, A.F., Immerzeel, W.W., 2017. Impact of a global temperature rise of 1.5 degrees celsius on Asia's glaciers. Nature. 549 (7671), 257–260. https://doi.org/10.1038/nature23878.
Kropáček, J., Neckel, N., Bauder, A., 2014. Estimation of mass balance of the grosser Aletschgletscher, Swiss Alps, from ICESat laser altimetry data and digital elevation models. Remote Sens. 6 (6), 5614–5632. https://doi.org/10.3390/rs6065614.
Kulkarni, A., Sabin, T.P., Chowdary, J.S., Rao, K.K., Priya, P., Gandhi, N., Bhaskar, P., Buri, V.K., Sabade, S.S., Pai, D.S., Ashok, K., Mitra, A.K., Niyogi, D., Rajeevan, M.,

2020. Precipitation changes in India. In: Krishnan, R., Sanjay, J., Gnanaseelan, C., Mujumdar, M., Kulkarni, A., Chakraborty, S. (Eds.), Assessment of Climate Change over the Indian Region. Springer, Singapore, pp. 47–72.
Kulkarni, A.V., Shirsat, T.S., Kulkarni, A., Negi, H.S., Bahuguna, I.M., Thamban, M., 2021. State of Himalayan cryosphere and implications for water security. Water Secur. 14, 100101. https://doi.org/10.1016/j.wasec.2021.100101.
Kumar, G.V., Kulkarni, A.V., Gupta, A.K., Sharma, P., 2017a. Mass balance estimation using geodetic method for glaciers in Baspa Basin, Western Himalaya. Curr. Sci. 113 (3), 486–492.
Kumar, V., Mehta, M., Mishra, A., Trivedi, A., 2017b. Temporal fluctuations and frontal area change of Bangni and Dunagiri glaciers from 1962 to 2013, Dhauliganga Basin, Central Himalaya, India. Geomorphology. 284, 88–98. https://doi.org/10.1016/j.geomorph.2016.12.012.
Lejeune, Y., Bertrand, J., Wagnon, P., Morin, S., 2013. A physically based model of the year-round surface energy and mass balance of debris-covered glaciers. J. Glaciol. 59 (214), 327–344. https://doi.org/10.3189/2013JoG12J149.
Lenderink, G., van Meijgaard, E., 2008. Increase in hourly precipitation extremes beyond expectations from temperature changes. Nat. Geosci. 1, 511–514. https://doi.org/10.1038/ngeo262.
Mcgrath, D., Sass, L., O'Neel, S., Arendt, A., Kienholz, C., 2017. Hypsometric control on glacier mass balance sensitivity in Alaska and Northwest Canada. Earths Fut. 5 (3), 324–336. https://doi.org/10.1002/2016EF000479.
McNabb, R., Nuth, C., Kääb, A., Girod, L., 2019. Sensitivity of glacier volume change estimation to DEM void interpolation. Cryosphere 13, 895–910. https://doi.org/10.5194/tc- 13-895-2019.
Meier, M.F., Post, A., 1969. What are glacier surges? Can. J. Earth Sci. 6 (4), 807–817. https://doi.org/10.1139/e69-08.
Mishra, A., Nainwal, H.C., Bolch, T., Shah, S.S., Shankar, R., 2022. Glacier inventory and glacier changes (1994-2020) in the Upper Alaknanda Basin, Central Himalaya. J. Glaciol. 1–16 https://doi.org/10.1017/jog.2022.87.
Mukherjee, K., Bolch, T., Goerlich, F., Kutuzov, S., Osmonov, A., Pieczonka, T., Shesterova, I., 2017. Surge-type glaciers in the Tien Shan (Central Asia). Arct. Antarct. Alp. Res. 49 (1), 147–171. https://doi.org/10.1657/AAAR0016-021.
Mukherjee, K., Bhattacharya, A., Pieczonka, T., Ghosh, S., Bolch, T., 2018. Glacier mass budget and climate reanalysis data indicate a climatic shift around 2000 in Lahaul-Spiti, western Himalaya. Clim. Chang. 148 (1), 219–233. https://doi.org/10.1007/s10584-018-2185-3.
Mukherjee, K., Menounos, B., Shea, J., Mortezapour, M., Ednie, M., Demuth, M., 2022. Evaluation of surface mass-balance records using geodetic data and physically-based modelling, place and Peyto Glaciers, Western Canada. J. Glaciol. 1-18 https://doi.org/10.1017/jog.2022.83.
Muñoz-Sabater, J., Dutra, E., Agustí-Panareda, A., Albergel, C., Arduini, G., Balsamo, G., Boussetta, S., Choulga, M., Harrigan, S., Hersbach, H., Martens, B., Miralles, D.G., Piles, M., Rodriguez-Fernandez, N.J., Zsoter, E., Buontempo, C., Thepaut, J.N., 2021. ERA5-land: a state-of-the-art global reanalysis dataset for land applications. Earth. Syst. Sci. Data. 13 (9), 4349–4383. https://doi.org/10.5194/essd-13-4349-2021.
Murray, T., Stuart, G.W., Miller, P.J., Woodward, J., Smith, A.M., Porter, P.R., Jiskoot, H., 2000. Glacier surge propagation by thermal evolution at the bed. J. Geophys. Res. Solid Earth 105 (B6), 13491–13507. https://doi.org/10.1029/2000JB900066.
Nainwal, H.C., Negi, B.D.S., Chaudhary, M., Sajwan, K.S., Gaurav, A., 2008. Temporal changes in rate of recession: Evidences from Satopanth and Bhagirath Kharak Glaciers, Uttarakhand, using total station survey. Curr. Sci. 94 (5), 653–660.
Nefian, A.V., Husmann, K., Broxton, M., To, V., Lundy, M., Hancher, M.D., 2009. A Bayesian formulation for sub-pixel refinement in stereo orbital imagery. In: 2009 16th IEEE International Conference on Image Processing (ICIP). IEEE, pp. 2361–2364.
Nuth, C., Kääb, A., 2011. Co-registration and bias corrections of satellite elevation data sets for quantifying glacier thickness change. Cryosphere. 5 (1), 271–290. https://doi.org/10.5194/tc-5-271-2011.
Østrem, G., 1959. Ice melting under a thin layer of moraine, and the existence of ice cores in moraine ridges. Geograf. Ann. Ser. A 41, 228–230.
Pandey, A., Garg, P.K., Nainwal, H.C., Rathore, B.P., Bahuguna, I.M., 2022. Comparative assessment of two neighbouring glaciers (Raj Bank and Kosa), Dhauliganga Basin, central Himalaya, India, since 1962 to 2019. J. Earth. Syst. Sci. 131, 214. https://doi.org/10.1007/s12040-022-01962-6.
Paul, F., Haeberli, W., 2008. Spatial variability of glacier elevation changes in the swiss alps obtained from two digital elevation models. Geophys. Res. Lett. 35 (21) https://doi.org/10.1029/2008GL034718.
Paul, F., Kääb, A., Maisch, M., Kellenberger, T., Haeberli, W., 2004. Rapid disintegration of Alpine glaciers observed with satellite data. Geophys. Res. Lett. 31 (2) https://doi.org/10.1029/2004GL020816.
Pfeffer, W.T., Arendt, A.A., Bliss, A., Bolch, T., Cogley, J.G., Gardner, A.S., Jon-Ove, H., Hock, R., Kaser, G., Kienholz, C., Miles, E.S., Moholdt, G., Mölg, N., Paul, F., Radic, V., Rastner, P., Raup, B.H., Rich, J., Sharp, M.J., The Randolph Consortium, 2014. The Randolph Glacier Inventory: a globally complete inventory of glaciers. J. Glaciol. 60 (221), 537–552. https://doi.org/10.3189/2014JoG13J176.
Phan, V.H., Lindenbergh, R.C., Menenti, M., 2014. Orientation dependent glacial changes at the Tibetan Plateau derived from 2003–2009 ICESat laser altimetry. Cryosphere Discuss. 8, 2425–2463. https://doi.org/10.5194/tcd-8-2425-2014.
Pieczonka, T., Bolch, T., 2015. Region-wide glacier mass budgets and area changes for the Central Tien Shan between~ 1975 and 1999 using Hexagon KH-9 imagery. Glob. Planet. Chang. 128, 1–13. https://doi.org/10.1016/j.gloplacha.2014.11.014.
Pieczonka, T., Bolch, T., Junfeng, W., Shiyin, L., 2013. Heterogeneous mass loss of Glaciers in the Aksu-Tarim Catchment (Central Tien Shan) revealed by 1976 KH-9 Hexagon and 2009 SPOT-5 stereo imagery. Remote Sens. Environ. 130, 233–244. https://doi.org/10.1016/j.rse.2012.11.020.
Pritchard, H.D., 2019. Asia's shrinking glaciers protect large populations from drought stress. Nature. 569 (7758), 649–654. https://doi.org/10.1038/s41586-019-1240-1.
Quincey, D.J., Luckman, A., 2014. Brief communication: on the magnitude and frequency of khurdopin glacier surge events. Cryosphere 8 (2), 571–574. https://doi.org/10.5194/tc-8-571-2014.
Quincey, D.J., Richardson, S.D., Luckman, A., Lucas, R.M., Reynolds, J.M., Hambrey, M. J., Glasser, N.F., 2007. Early recognition of glacial lake hazards in the Himalaya using remote sensing datasets. Glob. Planet. Chang. 56 (1–2), 137–152. https://doi.org/10.1016/j.gloplacha.2006.07.013.
Rabatel, A., Dedieu, J.P., Vincent, C., 2016. Spatio-temporal changes in glacier-wide mass balance quantified by optical remote sensing on 30 glaciers in the French Alps for the period 1983–2014. J. Glaciol. 62 (236), 1153–1166. https://doi.org/10.1017/jog.2016.113.
Racoviteanu, A., Arnaud, Y., Williams, M., Manley, W.F., 2014. Spatial patterns in glacier area and elevation changes from 1962 to 2006 in the monsoon-influenced eastern Himalaya. Cryosphere Discuss. 8 (4), 3949–3998. https://doi.org/10.5194/tcd-8-3949-2014.
Racoviteanu, A.E., Arnaud, Y., Williams, M.W., Manley, W.F., 2015. Spatial patterns in glacier characteristics and area changes from 1962 to 2006 in the Kanchenjunga–Sikkim area, eastern Himalaya. Cryosphere 9 (2), 505–523. https://doi.org/10.5194/tc-9-505-2015.
Ragettli, S., Bolch, T., Pellicciotti, F., 2016. Heterogeneous glacier thinning patterns over the last 40 years in Langtang Himal, Nepal. Cryosphere 10 (5), 2075–2097. https://doi.org/10.5194/tc-10-2075-2016.
Remya, S.N., Kulkarni, A.V., Syed, T.H., Nainwal, H.C., 2020. Glacier mass loss in the Alaknanda Basin, Garhwal Himalaya on a decadal scale. Geocarto. Int. 37 (10), 3014–3032. https://doi.org/10.1080/10106049.2020.1844309.
Remya, S.N., Syed, T.H., Kulkarni, A.V., Anand, R., 2022. Manifestation of topography and climate variations on long-term glacier changes in the Alaknanda Basin of Central Himalaya, India. Geocart. Int. 37 (26), 11010–11029. https://doi.org/10.1080/10106049.2022.2044392.
Rolstad, C., Haug, T., Denby, B., 2009. Spatially integrated geodetic glacier mass balance and its uncertainty based on geostatistical analysis: application to the Western Svartisen Ice Cap, Norway. J. Glaciol. 55 (192), 666–680. https://doi.org/10.3189/002214309789470950.
Rounce, D.R., Khurana, T., Short, M.B., Hock, R., Shean, D.E., Brinkerhoff, D.J., 2020. Quantifying parameter uncertainty in a large-scale glacier evolution model using bayesian inference: application to high mountain Asia. J. Glaciol. 66 (256), 175–187. https://doi.org/10.1017/jog.2019.91.
Rounce, D.R., Hock, R., McNabb, R.W., Millan, R., Sommer, C., Braun, M.H., et al., 2021. Distributed global debris thickness estimates reveal debris significantly impacts glacier mass balance. Geophys. Res. Lett. 48 https://doi.org/10.1029/2020GL091311 e2020GL091311.
Rowan, A.V., Egholm, D.L., Quincey, D.J., Glasser, N.F., 2015. Modelling the feedbacks between mass balance, ice flow and debris transport to predict the response to climate change of debris-covered glaciers in the Himalaya. Earth Planet. Sci. Lett. 430 (C), 427–438. https://doi.org/10.1016/j.epsl.2015.09.004.
Rowan, A.V., Egholm, D.L., Quincey, D.J., Hubbard, B., King, O., Miles, E.S., Miles, K.E., Hornsey, J., 2021. The role of differential ablation and dynamic detachment in driving accelerating mass loss from a debris-covered Himalayan glacier. J. Geophys. Res. Earth Surf. 126 https://doi.org/10.1029/2020JF005761 e2020JF005761.
Salerno, F., Thakuri, S., Tartari, G., Nuimura, T., Sunako, S., Sakai, A., Fujita, K., 2017. Debris-covered glacier anomaly? Morphological factors controlling changes in the mass balance, surface area, terminus position, and snow line altitude of Himalayan glaciers. Earth Planet. Sci. Lett. 471, 19–31. https://doi.org/10.1016/j.epsl.2017.04.039.
Saydi, M., Ding, J.L., 2020. Impacts of topographic factors on regional snow cover characteristics. Water Sci. Eng. 13 (3), 171–180. https://doi.org/10.1016/j.wse.2020.09.002.
Scherler, D., Bookhagen, B., Strecker, M., 2011. Spatially variable response of Himalayan glaciers to climate change affected by debris cover. Nat. Geosci. 4, 156–159. https://doi.org/10.1038/ngeo1068.
Sevestre, H., Benn, D., 2015. Climatic and geometric controls on the global distribution of surge-type glaciers: implications for a unifying model of surging. J. Glaciol. 61 (228), 646–662. https://doi.org/10.3189/2015JoG14J136.
Sevestre, H., Benn, D.I., Hulton, N.R.J., Baelum, K., 2015. Thermal structure of svalbard glaciers and implications for thermal switch models of glacier surging. J. Geophys. Res. Solid Earth 120 (10), 2220–2236. https://doi.org/10.1002/2015JF003517.
Shah, S.S., Banerjee, A., Nainwal, H.C., Shankar, R., 2019. Estimation of the total sub-debris ablation from point-scale ablation data on a debris-covered glacier. J. Glaciol. 65 (253), 759–769. https://doi.org/10.1017/jog.2019.48.
Sharp, M., Lawson, W., Anderson, R.S., 1988. Tectonic processes in a surge-type glacier. J. Struct. Geol. 10 (5), 499–515. https://doi.org/10.1016/0191-8141(88)90037-5.
Shean, D.E., Alexandrov, O., Moratto, Z.M., Smith, B.E., Joughin, I.R., Porter, C., Morin, P., 2016. An Automated, open-source pipeline for mass production of Digital Elevation Models (DEMs) from very-high-resolution commercial stereo satellite imagery. ISPRS J. Photogramm. Remote Sens. 116, 101–117. https://doi.org/10.1016/j.isprsjprs.2016.03.012.
Shean, D.E., Bhushan, S., Montesano, P., Rounce, D.R., Arendt, A., Osmanoglu, B., 2020. A systematic, regional assessment of high mountain Asia glacier mass balance. Front. Earth Sci. 7, 363. https://doi.org/10.3389/feart.2019.00363.
Shekhar, M.S., Chand, H., Kumar, S., Srinivasan, K., Ganju, A., 2010. Climate-change studies in the Western Himalaya. Ann. Glaciol. 51 (54), 105–112. https://doi.org/10.3189/172756410791386508.

Shen, C., Jia, L., Ren, S., 2022. Inter-and intra-annual glacier elevation change in high mountain Asia region based on ICESat-1&2 data using elevation-aspect bin analysis method. Remote Sens. 14 (7), 1630. https://doi.org/10.3390/rs14071630.

Shrestha, A.B., Aryal, R., 2011. Climate change in Nepal and its impact on Himalayan glaciers. Reg Environ Change 11 (Suppl 1), 65–77. https://doi.org/10.1007/s10113-010-0174-9.

Shukla, A., Qadir, J., 2016. Differential response of glaciers with varying debris cover extent: evidence from changing glacier parameters. Int. J. Remote Sens. 37 (11), 2453–2479. https://doi.org/10.1080/01431161.2016.1176272.

Singh, O., Arya, P., Chaudhary, B.S., 2013. On rising temperature trends at Dehradun in Doon Valley of Uttarakhand, India. J. Earth. Syst. Sci. 122 (3), 613–622. https://doi.org/10.1007/s12040-013-0304-0.

Steiner, J.F., Kraaijenbrink, P.D.A., Jiduc, S.G., Immerzeel, W.W., 2018. Brief communication: The Khurdopin glacier surge revisited – extreme flow velocities and formation of a dammed lake in 2017. Cryosphere 12 (1), 95–101. https://doi.org/10.5194/tc-12-95-2018.

Strozzi, T., Luckman, A., Murray, T., Wegmuller, U., Werner, C.L., 2002. Glacier motion estimation using SAR offset-tracking procedures. IEEE Trans. Geosci. Remote Sens. 40 (11), 2384–2391. https://doi.org/10.1109/TGRS.2002.805079.

Thayyen, R.J., Gergan, J.T., 2010. Role of glaciers in watershed hydrology: a preliminary study of a Himalayan catchment. Cryosphere. 4 (1), 115–128. https://doi.org/10.5194/tc-4-115-2010.

Vijay, S., Braun, M., 2016. Elevation change rates of glaciers in the Lahaul-Spiti (Western Himalaya, India) during 2000-2012 and 2012-2013. Remote Sens. 8 (12), 1038. https://doi.org/10.3390/rs8121038.

Vincent, C., 2002. Influence of climate change over the 20th century on four French glacier mass balances. J. Geophys. Res. Atmos. 107 (D19) https://doi.org/10.1029/2001JD000832. ACL4–1 – ACL4–12.

Viviroli, D., Archer, D.R., Buytaert, W., Fowler, H.J., Greenwood, G.B., Hamlet, A.F., et al., 2011. Climate change and mountain water resources: overview and recommendations for research, management and policy. Hydrol. Earth Syst. Sci. 15 (2), 471–504. https://doi.org/10.5194/hess-15-471-2011.

Zemp, M., Huss, M., Thibert, E., Eckert, N., McNabb, R., Huber, J., Barandun, M., Machguth, H., Nussbaumer, S.U., Gartner-Roer, I., Thomson, L., Paul, F., Maussion, F., Kutuzov, S., Cogley, J.G., 2019. Global glacier mass changes and their contributions to sea-level rise from 1961 to 2016. Nature. 568, 382–386. https://doi.org/10.1038/s41586-019-1071-0.

Zhao, H., Yang, W., Yao, T., Tian, L., Xu, B., 2016. Dramatic mass loss in extreme high-elevation areas of a western Himalayan glacier: observations and modeling. Sci. Rep. 6, 30706. https://doi.org/10.1038/srep30706.